Jussi Tikkanen

Use of Independent Sideband Modulation for Tactical Data Links

Metropolia University of Applied Sciences

Bachelor of Engineering

Information Technology

Bachelor's Thesis

15 March 2024

Abstract

Author:	Jussi Tikkanen
Title:	Use of Independent Sideband modulation for Tactical Data Links
Number of Pages:	59 pages + 2 appendices
Date:	March 15th, 2024
Degree:	Bachelor of Engineering
Degree Programme:	Information technology
Professional Major:	
Supervisors:	Janne Salonen, Principal Lecturer

The thesis evaluates the usability of independent sideband (ISB) modulation in wireless communication. The modulation is examined as part of a simulated HF frequency band tactical data link system, adhering to the specifications of the 3 kHz bandwidth waveform defined in MIL-STD-188-110D.

The performance of ISB is compared against single sideband (SSB) modulation with the same defined parameters from MIL-STD-188-110D. Evaluation criteria include the power loss and the increased throughput from two independent sidebands.

Two channel performance tests were conducted, and radio power output was measured with the waveform. The channel tests were performed under real-life conditions at northern geomagnetic latitudes, with the first test in November and the second test in February.

Tests were performed in varying wireless channel conditions to provide sufficient data for the erratic HF band. With these results, the usability of ISB waveforms can be compared to SSB waveforms.

The thesis describes multiple phenomena affecting signals in the HF frequency band in both ground wave and skywave propagation. This provides insight into the complex detrimental effects and unexpected, often rapid changes in the HF frequency band.

Keywords: Analog modulation, High Frequency, Independent sideband, ISB, Wireless communications, Ionosphere, Skywave propagation

---

Tiivistelmä

Tekijä:	Jussi Tikkanen
Otsikko:	Use of Independent Sideband modulation for Tactical Data Links
Sivumäärä:	59 sivua + 2 liitettä
Aika:	15.3.2024
Tutkinto:	Insinööri (AMK)
Tutkinto-ohjelma:	Tieto- ja viestintätekniikan tutkinto-ohjelma
Ammatillinen pääaine:	
Ohjaajat:	Osaamisaluejohtaja Janne Salonen

Tässä insinöörityössä arvioidaan toisistaan riippumattomien sivunauhojen (ISB) modulaation käytettävyyttä langattomassa tiedonsiirrossa. Modulaatio on osana simuloitua HF taajuusalueen taktista datalinkkiä, joka noudattaa MIL-STD-188-110D mukaista 3 kHz kaistanlevyisen aaltomuodon määritteitä.

Työssä verrataan ISB suorituskykyä yhden sivunauhan (SSB) modulaatiota vasten. Arvioinnin perusteina ovat ISB:n kahden sivunauhan lähetystehon menetys ja kasvu tiedonsiirtonopeudessa.

Testissä on toteutettu kaksi HF kanavamittausta sekä radion lähetystehon mittaus aaltomuodolla. Kanavamittaukset ovat toteutettu oikeissa olosuhteissa pohjoisen geomagneettisilla leveysasteilla, joista ensimmäinen marraskuussa ja toinen helmikuussa.

Kahdella toisistaan eriävällä radiokelillä tehdystä mittauksesta voidaan muodostaa riittävä arvio ailahtelevasta radiotaajuusalueesta ja eri ISB aaltomuotojen käytettävyydestä.

Työssä kuvataan HF taajuusalueen signaaliin vaikuttavia ilmiöitä pinta- ja avaruusaallossa. Tällä selkeytetään monimuotoisia haittaavia vaikutuksia ja yllättäviä sekä nopeita muutoksia, mitä HF taajuusalueella ilmenee.

Avainsanat: Analoginen modulaatio, HF, Toisistaan riippumattomat sivunauhat, ISB, Langaton tiedonsiirto, Ionosfääri, Avaruusaalto

Contents

Appendices

Appendix 1: Ionospheric conditions during the testing periods

Appendix 2: Radio power output measurement

List of Abbreviations

AGC:	Automatic gain control
ALE:	Automatic Link Establishment
AM:	Amplitude modulation
AWGN:	Additive white gaussian noise
BER:	Bit error rate
BLOS:	Beyond Line-of-Sight
CME:	Coronal mass ejection
dB:	Decibel (dBi: isotropic antenna, dBm: decibel-milliwatts)
DSB:	Double sideband
FC:	Full carrier, used in conjunction with analog modulation
HF:	High frequency
HPBW:	Half-power beamwidth
Hz:	Hertz, a unit of frequency
ISB:	Independent sideband
ITM:	Irregular terrain model
ITU:	International Telecommunication Union
ITU-R:	ITU Radiocommunication sector

LSB: Lower sideband

LUF: Lowest usable frequency

MF: Medium frequency

MUF: Maximum usable frequency

NVIS: Near vertical incidence skywave

RF: Radio frequency

RMS: Root Mean Square

RSSI: Received signal strength indicator

SC: Suppressed carrier, used in conjunction with analog modulation

SDR: Software defined radio

SID: Sudden ionosphere disturbance

SNR: Signal-to-noise ratio

USB: Upper sideband

TDM: Time division multiplexing

TDMA: Time division multiple access

TIREM: Terrain integrated rough Earth model

VOACAP: Voice of America coverage analysis program’

W: Watt, unit of power

1 Introduction

The ability to communicate orders and relay situational awareness has always been imperative for success on the battlefield, from the use of runners to satellite communication. Ever since radio equipment was harnessed in military use, it has played an important role in coordinating the order of battle. This role keeps expanding constantly as the technology improves.

Tactical data links have become a mainstay to disseminate data from various sensors and distribute it to all units participating in the network [1, p. 1-1]. This information can be distributed via wired or wireless communication means.

In BLOS wireless communication, the only options available are HF and satellite communications. Satellites may not always be available due to the high cost and vulnerability. Uplink jamming, which can be enacted from a safe distance, can prevent or limit the use of a satellite, particularly for geostationary satellites [2, p. 217].

HF communications have become again prevalent as an option for BLOS communication. However, due to the limits imposed by physics on an HF signal the throughput cannot be compared to satellite communication. The current limits of the throughput for any given digital modulation can be improved, by expanding the bandwidth of the signal or by using both sidebands to transmit independent information.

This thesis aims to inspect the usability of ISB signals to increase the throughput of simulated tactical data links, which follow the MIL-STD-188-110D guidelines. It will include the analysis of ionospheric and ground wave propagation paths.

The main factors will be the signal strength on fixed power output for an ISB compared to SSB transmissions against the potential gain from throughput. This includes measurements of two diverse channel conditions.

2 Wireless signal

Wireless signals are transmissions between transmitter and receiver, where electromagnetic waves travel in a non-confined medium, such as air, vacuum, or seawater [3, p. 97]. These signals are also called unguided media or RF signals. The transmitter radiates the signal from an antenna to the receiver's antenna. The receiver might not be stationary, the transmission is radiated within the parameters of the antenna with no certainty it reaches the intended recipient.

The electromagnetic wave has two components: electric and magnetic fields. Electric charge shifts from end to end in an antenna resulting in a field that escapes the confines of the antenna, when negative and positive charges meet, this creates a current that creates a magnetic field [4, p. 10]. These fields oscillate perpendicularly to each other, towards the propagation direction, as depicted in Figure 1.

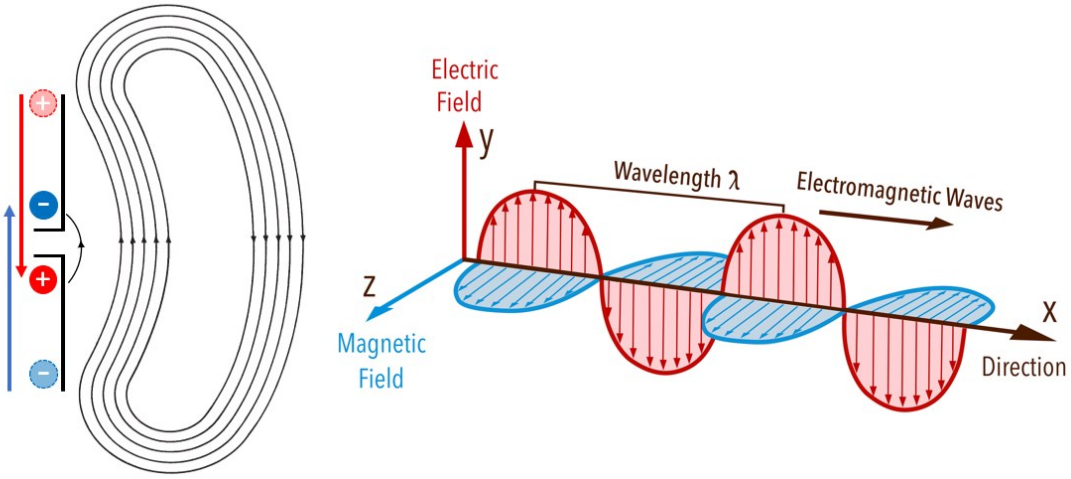

Figure 1. Electromagnetic field escaping antenna when electric poles shift and pass each other. On the right is a depiction of electromagnetic wave [5].

Signals are observed in two different domains, the more conventional time domain, where both desired and undesired signals mix. The other is the frequency domain where all received signals are separated to their respective

frequencies by using Fourier analysis. The frequency domain is the more relevant for signal analysis, as from it can be extracted the desired signal, peak amplitude, and bandwidth [3, p. 101].

2.1 Analog transmission

Wireless signals may contain either analog or digital data when transmitted, however, all wireless transmissions are analog [3, p. 114]. The original data is modulated and fitted with a carrier wave, which can be transmitted to the receiver where it can be demodulated and interpreted.

For data, baseband signal, to be transmitted over longer distances, it must be modulated. Modulation is a method to encode information into a carrier signal, where the carrier signal may be altered in amplitude, frequency, phase, or a combination of those [3, p. 174]. In Figure 2 are the parameters of the modulated signal: carrier signal, f_c, and two sidebands, upper, f_{USB}, and lower, f_{LSB}, combined f_m.

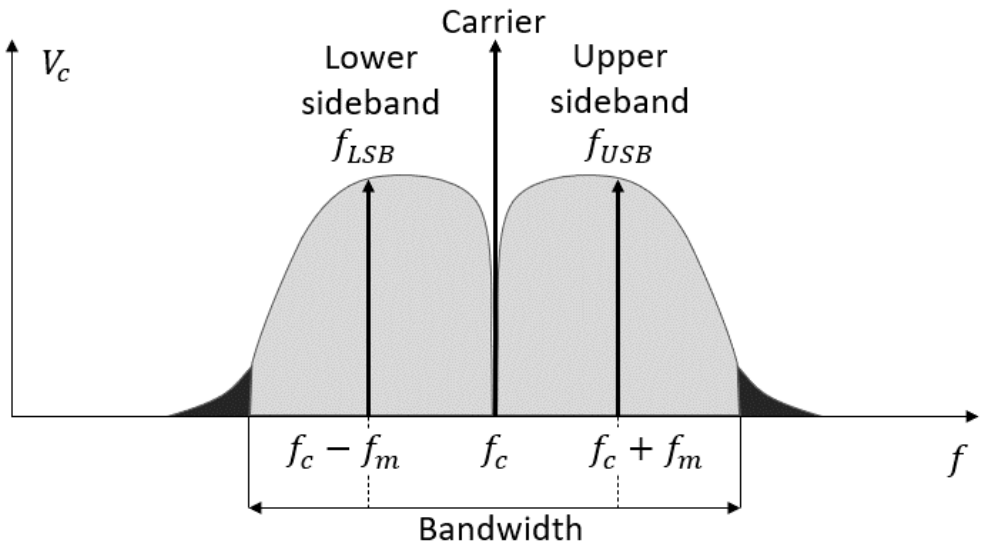

Figure 2. Depiction of the modulated signal, where all components are present: carrier, upper sideband, and lower sideband. Sideband arrows indicate controlled data transmission and grey shapes represent non-uniform information as the highest modulating frequency.

The modulated signal requires an equivalent space in the frequency spectrum as the frequency of the baseband signal, this is known as bandwidth, *B* [3, p. 101]. Bandwidth determines the boundaries of the transmitted signal in the frequency spectrum, if another signal crosses this part of the spectrum, it causes interference.

Depending on the modulated information the size of bandwidth increases. If the information is a tone or controlled data at a set frequency, say 300 Hz, then the bandwidth is +300 Hz and -300 Hz from the carrier frequency, a total of 600 Hz. However, if the information has broad and non-uniform content, such as human speech, the bandwidth will be determined by the highest modulating frequency.

2.2 Analog waveforms

AM is the first discovered and simplest modulation. From it many of the other modulations are derived, so it makes a good baseline to compare other modulations. AM has the carrier wave and both sidebands intact, it is often listed as DSB-FC or DSB-AM.

In AM the baseband signal is attached to the carrier so that it modifies its voltage peaks, causing the amplitude of the transmitted signal to vary in the time domain as seen in Figure 3 [6, p. 36]. The added shape is called the envelope, and it matches the baseband signal’s voltage peaks. At the receiver end, the envelope can be extracted from the signal by detecting the amplitude peaks by comparing difference from measured time.

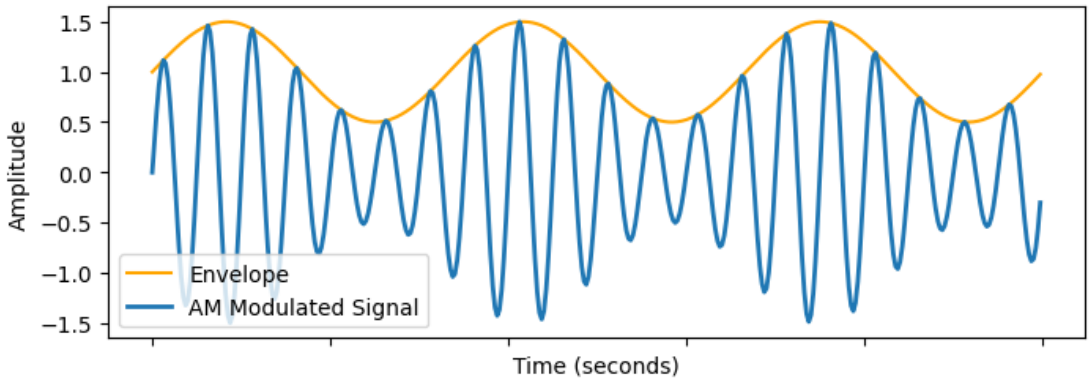

Figure 3. Amplitude modulation, the modulated carrier signal in blue and the envelope or message in orange.

AM modulated signals can be mathematically represented with Equation 1. Where $cos2\pi f_c t$ is the carrier wave and the two remaining segments of the equation stand for both sidebands, $cos2\pi(f_c-f_m)t$ and $cos2\pi(f_c+f_m)t$. The parameter A_m is the message, also known as the envelope.

$$s_{AM}(\mathrm{t}) = \cos 2\pi f_c t + \frac{A_m}{2}\cos 2\pi(f_c - f_m)t + \frac{A_m}{2}\cos 2\pi(f_c + f_m)t \qquad (1)$$

Equation 1. AM modulated signal [3, p. 527].

In frequency modulation, instead of manipulating the amplitude of the carrier, the intensity of the frequency varies according to the baseband signal [6, p. 80]. frequency modulation is directly comparable to AM's high and low amplitude peaks. When the intensity rises the message peak is reached, and at the lowest value, there is no data. In Figure 4 the effect of the sinewave message is implemented to the carrier wave resulting in the frequency modulated signal.

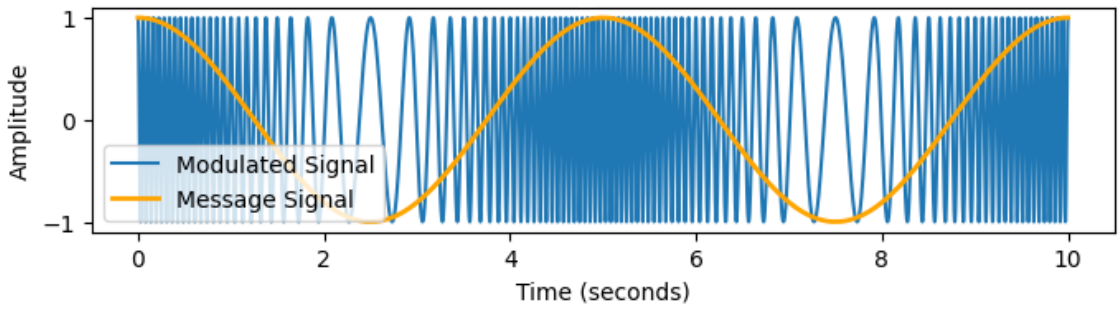

Figure 4. Frequency modulation. The intensity or rate of frequency increases the higher the message amplitude is.

Phase modulation expands to the features of frequency modulation; it varies the phase of the signal depending on the baseband signal, meaning that instead of amplitude, the angle of the signal changes [6, p. 89]. When the baseband signal turns from negative to positive or vice versa, the phase of the modulated signal deviates as seen in Figure 5.

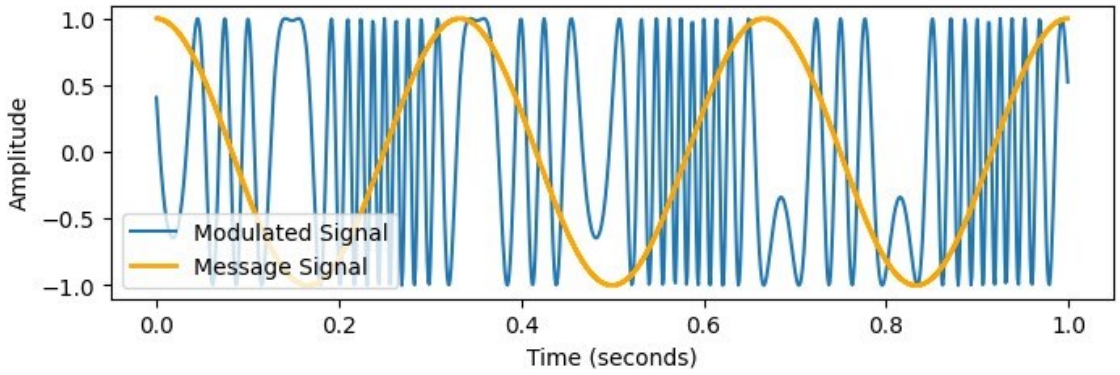

Figure 5. Phase modulation. When the message signal reaches a peak, the phase of the carrier signal changes.

In the following sub-chapters, the focus will be on band-pass filtered signals. The baseband signal that is modulated will be modified further by removing parts of the full product. This can include the carrier wave and either one of the sidebands.

2.2.1 Suppressing the carrier wave

The carrier wave has a sinusoidal component, which does not convey the message signal. As this component cannot be utilized for the benefit of modern wireless communications, the power is considered wasted [7, p. 6-1].

The carrier wave is suppressed, which is achieved by filtering this part of the signal. The carrier wave is suppressed at the transmitter, and it must be reconstructed at the receiver. Both the frequency and phase must be correct for the successful reception of the signal [8, p. 218].

In the following subchapters, all modulations have a suppressed carrier wave. This method increases the power efficiency of a transmission, which will be evaluated in Chapter 0.

2.2.2 Double sideband modulation

DSB-SC resembles an AM transmission, it has both upper and lower sidebands, but the carrier wave is removed. Like in AM, both sidebands contain identical information, resulting in a symmetrical representation in the frequency spectrum, Figure 6.

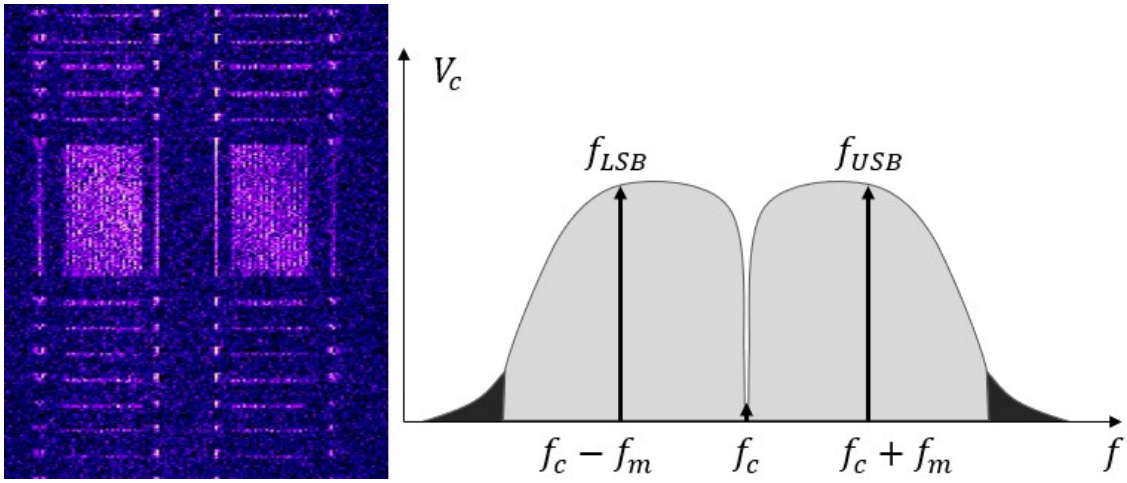

Figure 6. On the left is a spectrogram view of DSB-SC data transmission (LINK 11), both sidebands are symmetric [9]. On the right is a frequency domain

representation, without carrier wave, and both sidebands with identical information.

In Equation 2, a DSB modulated signal is mathematically represented. The calculation is similar to AM, the most evident differences are the missing carrier frequency and the A_m being replaced by half value, which is due to the power being divided to both sidebands equally.

$$s_{DSB}(\mathrm{t}) = \frac{1}{2}\cos 2\pi(f_c - f_m)t + \frac{1}{2}\cos 2\pi(f_c + f_m)t \quad (2)$$

Equation 2. DSB modulated signal [7, p. 6-2].

In DSB, the modulated information value can be positive or negative, which is visible in Figure 7. At the pass of the zero-point in amplitude the phase reverses 180 degrees. Therefore, AM demodulation or an envelope detector cannot be applied, a method known as coherent demodulation. This increases the complexity of the demodulation, as the lack of a carrier wave can lead to a phase error, which can cause heavy distortion to the demodulated signal [10, p. 115].

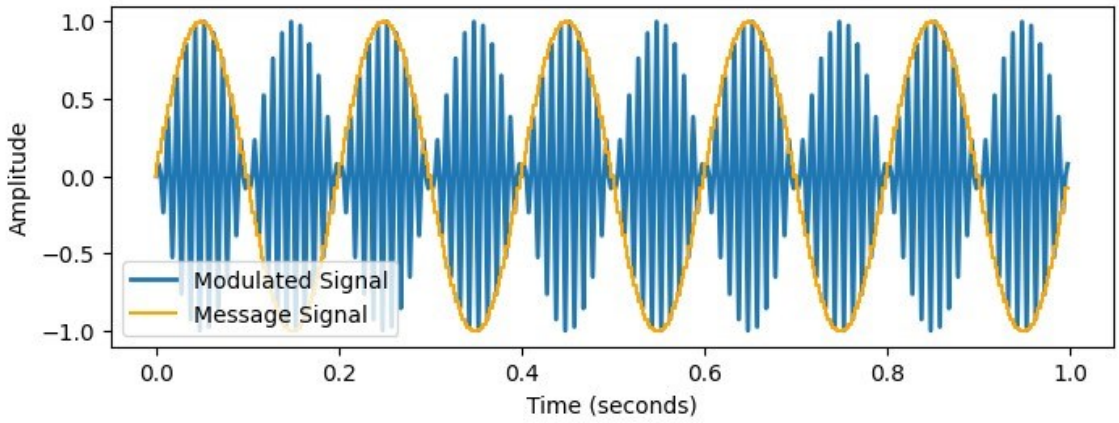

Figure 7. Time domain representation of DSB-SC.

Like in the AM signal, in DSB-SC the bandwidth requirement is double, *2B*, as both sidebands are present. The same information is transferred on both sidebands, this provides extra reliability if one of the sidebands cannot be received. DSB is regarded to be spectrally inefficient.

2.2.3 Single sideband modulation

Like DSB, SSB is a special type of AM. In DSB both sidebands carry identical information, so there is no data loss if one of them is suppressed. The data can be reconstructed from the remaining sideband without loss [10, p. 124]. It is notably more efficient to send a single sideband than both, but it also adds complexity to modulation and receiving the signal.

SSB-SC modulation is generated from DSB-SC with one of the sidebands filtered, as seen in Figure 8, resulting in a signal that requires a much narrower bandwidth than AM or DSB modulated signals [10, p. 125].

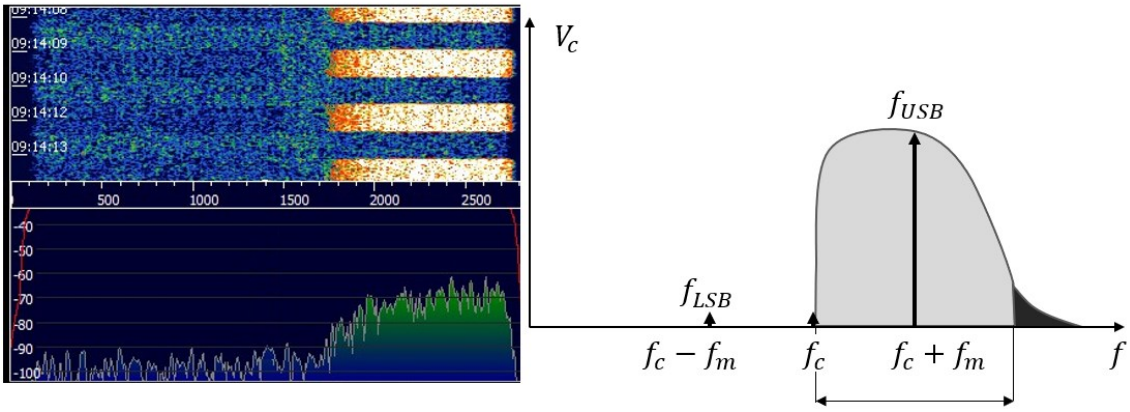

Figure 8. On the left a spectrogram view of a SSB-SC transmission. On the right a frequency domain depiction, both carrier and LSB are suppressed, reducing the required RF bandwidth to about half.

SSB can be represented mathematically, in Equation 3, both USB and LSB have different representations, known as the Hilbert transform. There also exist other methods to generate an SSB signal; phase-shift modulation [10, p. 127]. In both equations *s(t)* stands for the real value of the message and *ŝ(t)*

represents the Hilbert transform. If Equation 3 was LSB, the Hilbert transform would be added instead of subtracted.

$$s_{SSB}(\mathrm{t}) = s(t)\cos(2\pi f_c t) - \hat{\mathrm{s}}(t)\sin(2\pi f_c t) \quad (3)$$

Equation 3. Upper sideband modulated signal [10, p. 127].

Regardless of the filtering method, the same SSB signal is generated without discrepancies in the quality of the signal [6, p. 68]. Generally, the military uses USB. Radio amateurs often use LSB, but on occasion, they use USB, especially on over 10 MHz frequencies. From a technical point of view, there is no difference in which sideband is used.

When the transmission is received, the carrier wave must be reinserted to demodulate the signal correctly. If the frequency does not match the original carrier frequency, the information may be lost, as the filter does not align correctly. In the case of data transmission, the content can be lost completely and with voice transmissions, depending on the severity of misalignment, voices may be unintelligible or the pitch changes [11].

2.2.4 Independent sideband modulation

ISB modulation is in many ways identical to the DSB, but with a crucial difference: the information in each sideband is different: independent. With two unique sidebands, one on USB and the other on LSB, it can be viewed as two separate SSB transmissions on the same carrier wave, as depicted in Figure 9. This means that compared to DSB, it has twice the repetition rate of modulating signal frequency.

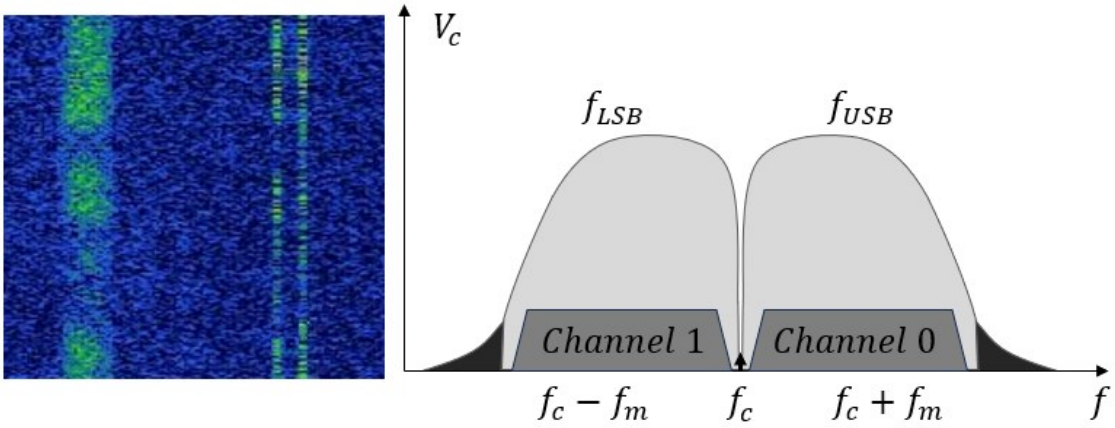

Figure 9. On the left is a spectrogram view of Modernised High Frequency Communication System (MHFCS), in USB there are two channels and LSB has one wider channel [12]. On the right is a frequency domain representation of a two-channel ISB.

The traditional ISB transmission system consists of two independent message channels which are driven in a separate line through filters, one for USB and the other for LSB. Both sidebands are modulated independently. These are then combined to form a signal. The system is described in Figure 10, the signal goes to a balanced mixer where it is combined to the desired transmission frequency [6, p. 72].

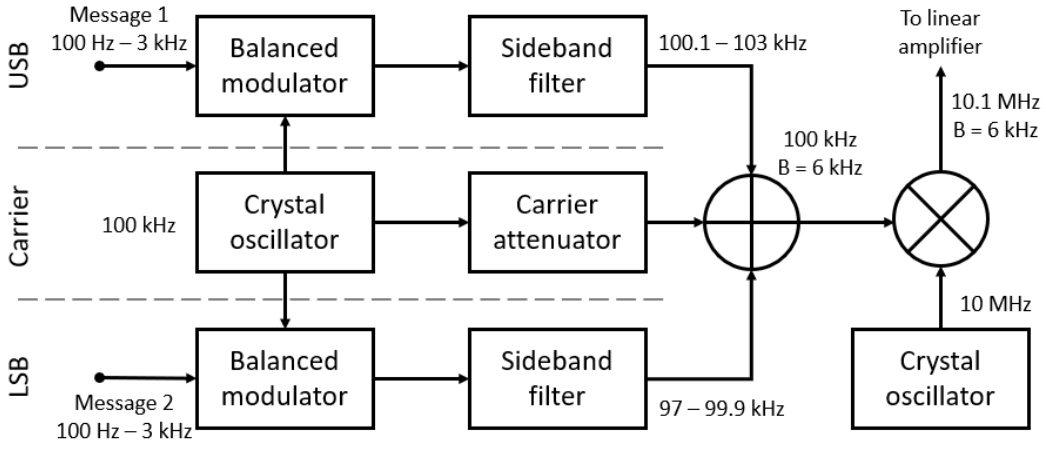

Figure 10. Traditional ISB system, where two independent messages with 3 kHz bandwidth are generated. Both sidebands are handled separately until added and mixed with the final frequency of 10MHz.

As the ISB can be viewed to be two unique sidebands sharing a carrier wave, it can be represented in the time domain as two independent SSB transmissions combined, as depicted in Figure 11. ISB is more affected by frequency distortion and phase instability compared to SSB, due to the nature of the signal.

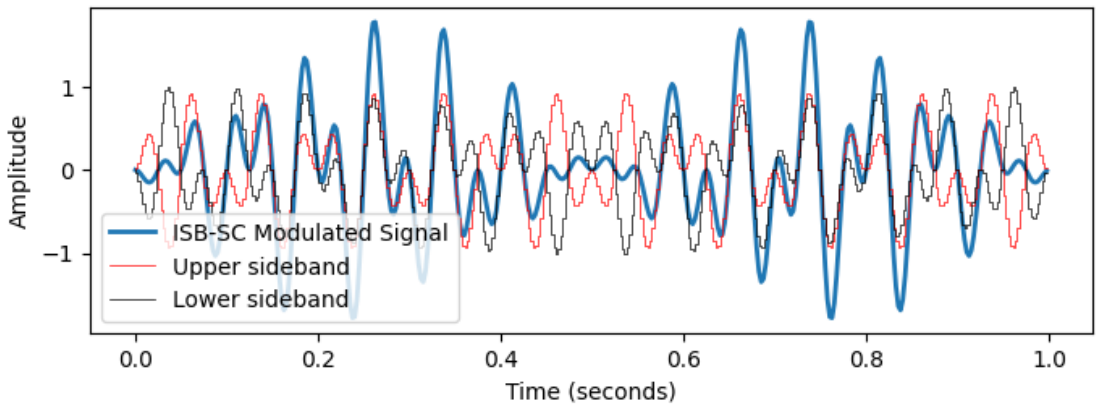

Figure 11. Time domain representation of ISB-SC.

ISB is still used for voice transmissions, but due to the complex system, it is rare these days. Data transmission applications for military use exist, the specifications are defined in the MIL-STD-188-110 and STANAG 4359. MIL-STD-188-141 also defines two separate modes: two- and four-channel ISB with 3 kHz bandwidth per channel [13, p. 4].

Both, MIL-STD-188-110 and STANAG 4359, define a more efficient method for generating ISB modulation with multiplexing. Multiplexing is a method of taking multiple sources and compressing them into a single output, and with ISB it would be accurate to state that this is an inverted process: demultiplexing to multiplexing.

The information is taken from a single source and spread to multiple outputs, Figure 12, dividing the information into their respective channels into both sidebands in a predefined pattern [14, p. 255]. Multiplexing is performed employing interleaving, this will divide the data approximately equally between

channels, starting from the higher frequency and moving down to lower frequencies, then repeating the cycle.

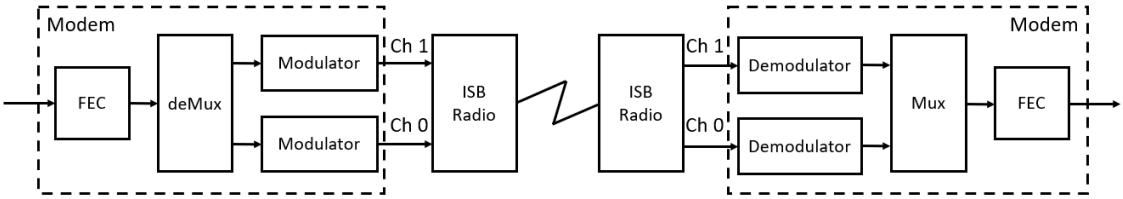

Figure 12. ISB modem and radio as defined in MIL-STD-188-110D [14, p. 258].

The increased number of channels in a transmission provides the possibility to use lower order modulation or lower modulation rate, while still maintaining higher throughput compared to DSB or SSB. Since the bandwidth increases from SSB to ISB, in other words the symbol rate will double when transmitting digital data, resulting in a higher throughput [14, p. 143].

Four-channel ISB is done by increasing the bandwidth to accommodate additional channels, in which two individual channels can reside within a sideband [6, p. 73]. Using this system will double the required bandwidth of the ISB signal.

Four-channel system increases the complexity of the waveform and may suffer more from frequency distortion. The system is not recognized by the STANAG 4539 and as such, while an interesting topic, shall not be explored further.

2.3 Analog modulation efficiency

The efficiency of analog modulation can be determined by the power efficiency and modulation index, *m*, as output power directly contributes to the field strength at the receiver.

The modulation index is the maximum depth of amplitude in a modulated carrier wave. The varying depth influences the power efficiency and increases the SNR

as the envelope detector has an easier task, thus providing more robust communication [6, p. 58]. Optimally modulation index may vary between 10–100%, anything over 100% will result in distortion, Figure 13.

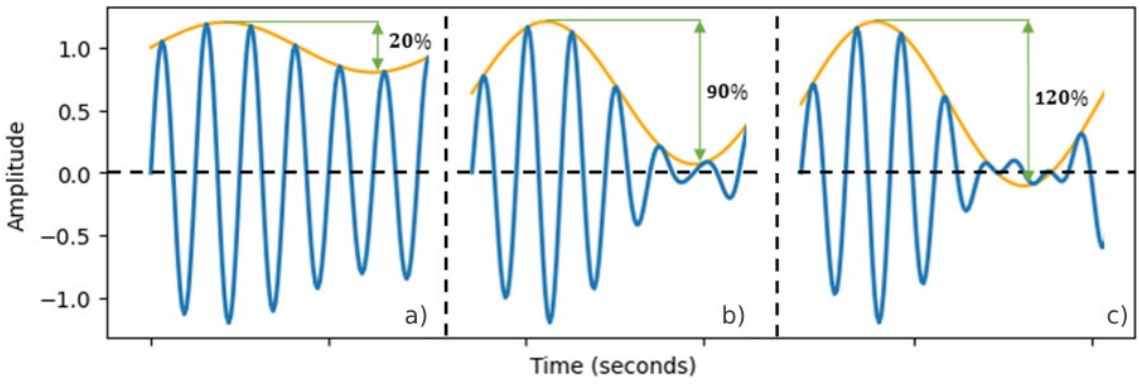

Figure 13. Three different modulation indexes. a) inefficient modulation with 20% index. b) efficient modulation index of 90%. c) overmodulation causes distortion and the information is lost.

The modulation index is achieved by adding or subtracting power on the carrier wave, the sidebands have varying amplitude, and the power of the carrier remains constant [15, p. 127]. The result of this is that in DSB-FC the carrier wave will always consume at least ⅔ of the total transmission power, Figure 14.

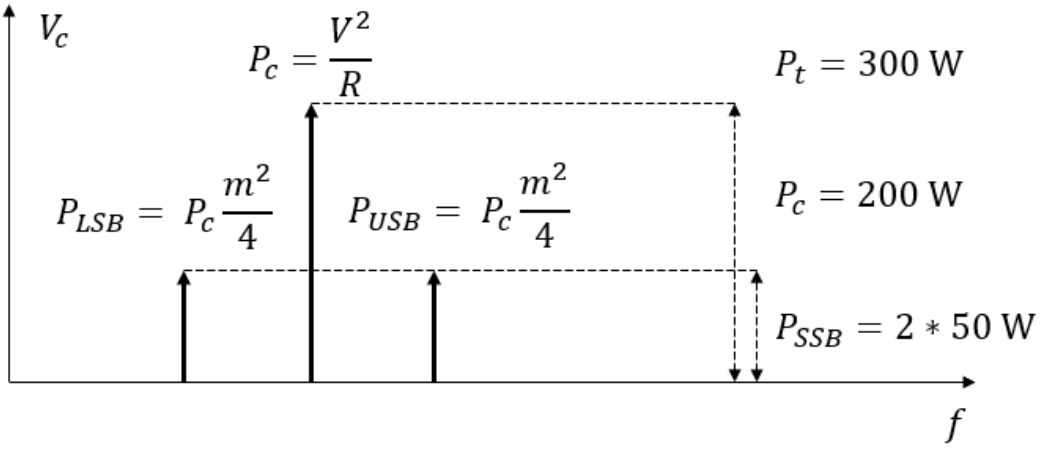

Figure 14. How power is divided by DSB-FC modulation. Of 300 W transmission power, the carrier requires 200 W and as both sidebands have the same information, the power used to transmit the message is 50 W.

The mathematical representation of power efficiency, η, can be broken down to A_c, which is the carrier wave amplitude and modulation index, m. This equation can be altered to fit DSB-SC and SSB, and ISB matches the DSB-SC.

$$\eta = \frac{useful\ power}{total\ power} = \frac{\frac{1}{4}m^2A_c^2}{\frac{1}{2}A_c^2 + \frac{1}{4}m^2A_c^2} = \frac{m^2}{2+m^2} \quad (4)$$

Equation 4. Power efficiency of transmitted DSB-FC signal [16, p. 80].

Any modulated signal with a carrier wave is extremely inefficient in modern communications. Better results will be obtained from suppressed carrier wave communications. Figure 15 shows DSB-SC and SSB-SC power efficiency.

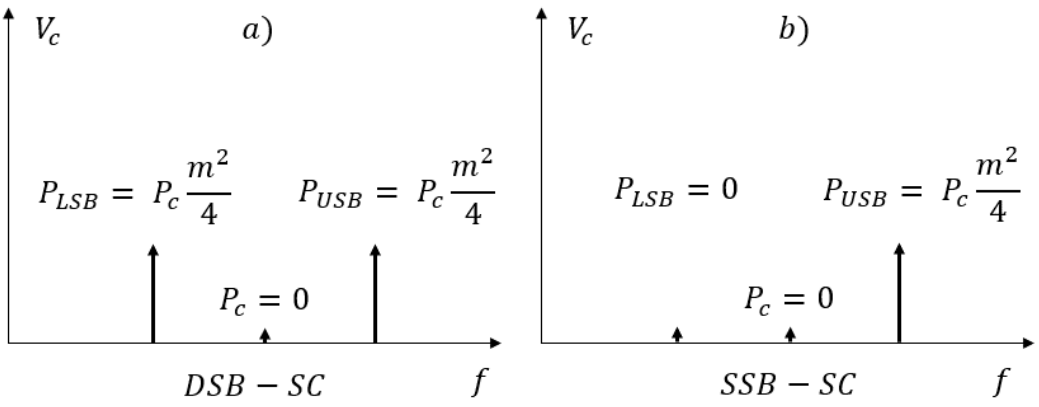

Figure 15. a) DSB-SC reached 50% power efficiency. If 300 W was to be used to transmit this message, the effective output is150 W. b) SSB-SC with 100% power efficiency, here the effective output is the full 300 W.

DSB has a theoretical efficiency of 50% because the modulated signal is doubled in two identical sidebands. SSB has a theoretical efficiency of 100% as only a single sideband remains, and all the power can be allocated to it. SSB is also more bandwidth efficient and as such desirable.

ISB is mathematically equivalent to DSB in this case, but the true significance lies in the data throughput efficiency as multiple messages can be transmitted simultaneously with each channel.

The evident benefit is on the SSB side. In wireless communication, the unit of measurement is decibel, *dB*. Since decibels are expressed in a logarithmic scale the difference of 50% transmission power is 3 dB, regardless of the amount of original power [17, p. 188].

3 HF communications

All wireless communications are based on electromagnetic waves, which can propagate in a free space, therefore not needing a medium for transmission. Their perpendicular binding towards the receiver antenna is what makes RF transmissions possible. The transmitted signal is subject to interference on the channel, this is known as noise, which is caused by natural and man-made sources [18, p. 1].

HF is a specific band within the RF spectrum spanning from 3 – 30 MHz. Occasionally this is expanded to the upper part of the MF band, increasing the band to 2 – 30 MHz [19, p. 1-6]. This will be the definition of the HF band in this thesis.

HF wavelength spans from 10 – 150 meters, where 2 MHz represents the longer wavelength and 30 MHz is the shorter. HF wavelength exhibits unique propagation properties compared to the higher RF bands, which makes the band ideal for BLOS communication.

In HF communications two distinct means of propagation increase the connection range: skywave and ground wave. Depending on the frequency and ionosphere conditions skywaves can refract from the ionosphere’s layers, thus increasing connection range up to thousands of kilometres. Ground wave has

an increased propagation distance over the horizon compared to line-of-sight propagation.

These properties make HF an appealing propagation method for maritime and military use, where distances are longer, and the use of satellites could be deemed too costly. The downside is reduced data throughput and rapidly changing ionospheric conditions due to effects from multiple sources, like solar activity.

With a skywave propagation the biggest problems come with choosing the right antenna and frequency, to avoid creating blind areas where establishing communications is desired. These blind areas between ground wave and skywave are known as skip zone, where communications cannot be established [20]. The frequency must be adjusted periodically to sustain the connection between stations to control the skip zone.

In Figure 16 are the two HF propagation methods, which will be used when comparing the use of ISB against SSB in this thesis. The ground wave propagates along the Earth's surface and skywave refracts from the ionosphere. There are other propagation methods, but these will not be the focus of this thesis.

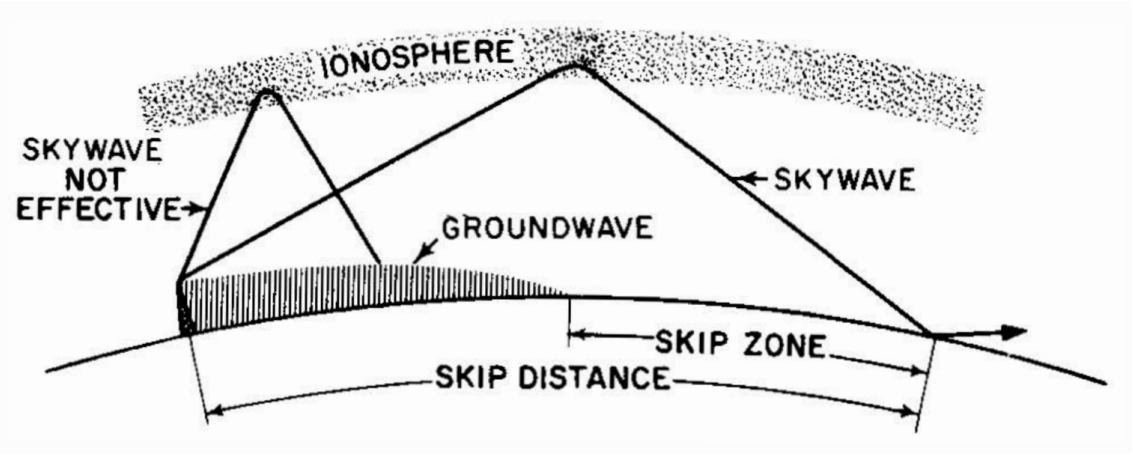

Figure 16. Oblique HF propagation and skip zone illustrated [21, p. 129]. Unlike in the picture, a sharp take-off angle is possible with proper antenna choice.

HF can also propagate through line-of-sight propagation, which will provide an optimal channel with minimal interference. This method of propagation might also experience reflected waves, which can have additive or destructive effects on the transmitted signal. However, it does not fall within the individualistic properties of HF propagation.

HF communication has served both civilian and military applications for over 100 years. In 1923, the U.S. Department of Commerce defined frequencies for government-specific use, including Navy and Air Force [22, pp. 9-13]. Since the dawn of satellite communications in the 1960's, communication satellites have been steadily replacing HF as a main long-range communication method [23, p. 15].

In the last decade, we have seen a gradual return to HF communications in software-defined radios and cognitive ALE, providing an evolution to faster and more reliable link establishment [24, p. 1].

3.1 Ground wave propagation

The ground wave propagates parallel to the ground, following the contours of the surface, until it gets absorbed or attenuated, by mixing into the background noise. This method of propagation is possible because longer wavelengths are more capable of diffracting around obstacles and contours.

Lower frequency waves propagate further parallel to the surface, reach is extended by the salinity and humidity of the surface [15, p. 32]. The range of the HF band most suited for ground wave propagation is 2 – 10 MHz, higher frequencies than that tend to distort the signal at longer distances [25, p. 195].

The three constants that affect the electrical characteristics of the surface are relative permeability, conductivity, and the dielectric constant [26, p. 23]. Ground waves remain relatively unaffected by atmospheric changes.

Ground wave polarization must be vertical. Horizontal polarization would be parallel to the Earth's surface, and it would short-circuit with the conductivity of the surface. The surface has resistance and acts as a lossy dielectric, which causes a wave to tilt towards the surface and eventually to attenuate, limiting the propagation distance [27, p. 50] [21, p. 122].

Sea water has a considerably higher conductivity than ground of any other type, as seen in **Virhe. Kirjanmerkin viittaus itseensä ei kelpaa.**. Combined with a near-vertical electric field of ground wave propagation we can achieve distances up to 200 – 300 km in maritime environments, on land the propagation distance is greatly reduced [28, p. 6]. Drastically lower salinity and cooler temperatures are defining factors in the Baltic Sea, and more so in the northern parts of it.

Table 1. Ground wave propagation constants for different surfaces [28, p. 10], which are valid for frequencies up to 30 MHz.

Description	Conductivity (S/m)	Relative permittivity compared to vacuum
Sea water, low salinity	1	80
Sea water, average salinity	5	80
Freshwater	0.003	80
Land	0.03	40
Wet ground	0.01	30
Land	0.003	22
Medium dry ground	0.001	15
Dry ground	0.0003	7
Very dry ground	0.0001	3
Fresh water ice, -1˚C	0.00003	3
Fresh water ice, -10˚C	0.00001	3

3.1.1 Sea surface propagation

Sea surface conductivity is dependent on the surface salinity and temperature. The conductivity (σ) of seawater can be calculated with Equation 5, where *C* is salinity (g/l), and *T* is the temperature (˚C) [28, p. 13].

$$\sigma = 0.18\mathrm{C}^{0.93}(1 + 0.02(T - 20)) \quad (5)$$

Equation 5. The conductivity of seawater [28, p. 13].

With Equation 5 we can calculate the values for conductivity in different ground types and gain an understanding of differences in various waterbodies around the world. All comparisons use a temperature of 18 ˚C as reference temperature, salinity is reported as average. Northern Baltic Sea has σ of 0.77 S/m, Eastern Atlantic Ocean has σ of 4.84 S/m and Mediterranean Sea has σ of 5.09 S/m.

Even if this is not the most accurate comparison due to the size of the water bodies, it still highlights the lower conductivity of the Baltic Sea, which reduces the maximum link establishment range to about 60 - 80 km. This range is still superior compared to line-of-sight propagation.

In Figure 17. we can see Eckert's theoretical model for calculating the distance an AM signal could travel on a smooth earth's surface [29]. It gives a theoretical signal field strength over a distance compared to the frequency. The values are set to represent late summer conditions in the Northern Baltic Sea and have been roughly adapted to a higher frequency range than the original simulation [30] [31].

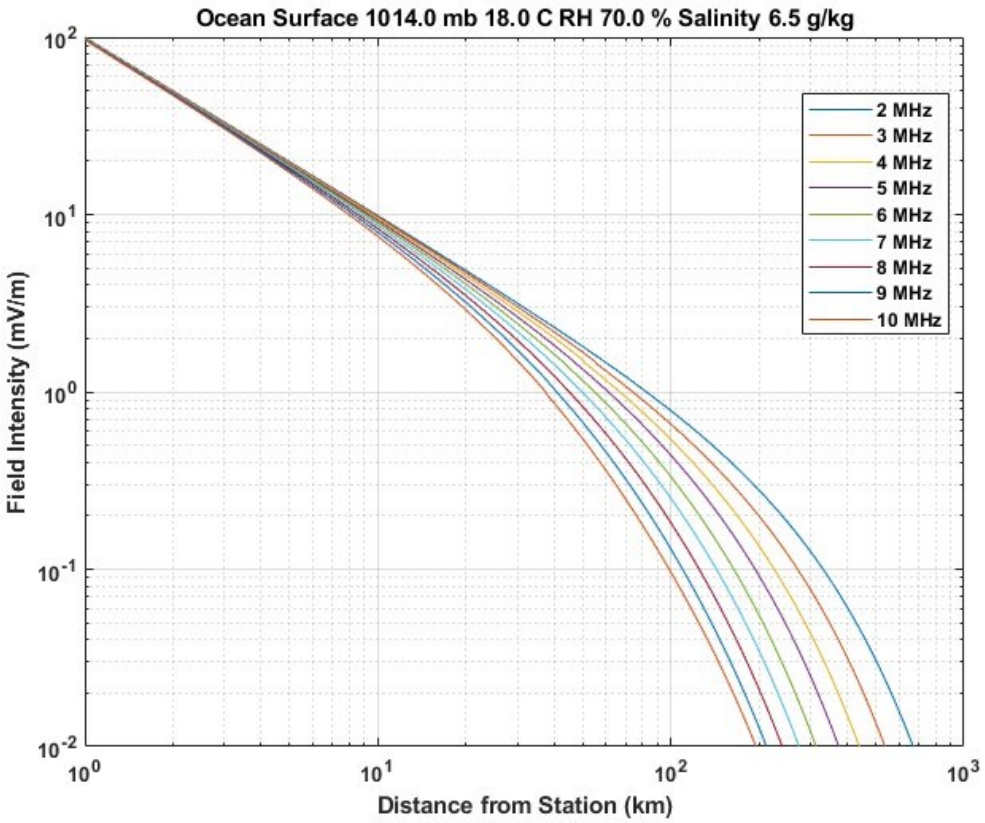

Figure 17. Simulated ground wave. The receiver's sensitivity defines the maximum reception range in conjunction with noise. The lower HF range is more inclined to ground wave propagation than the upper HF.

3.1.2 Homogeneous propagation model

It is complicated to predict ground wave propagation and multiple models exist exploring the problem, but the commonly used one is the Sommerfeld-Norton model. Additionally, the problem has been worked on by Van der Pol and Bremmer, who turned it suitable for engineering use [32, p. 127]. Norton further simplified it for practical use, but it still did not account for diffraction from Earth's curvature [28, p. 1].

Equation 6 is a simplified model proposed by Norton for ground wave attenuation, *F*, which is dependent on ground type and path length.

$$\mathrm{F} = \left[1 - j\sqrt{(\pi w)^{-w}\{erfc(j\sqrt{w})\}}\right] \quad (6)$$

Equation 6. Norton's attenuation function [28, p. 4].

In Equation 6 *erfc* is a complementary error function, and *w* is opened in Equation 7, where u^2 accounts for relative permittivity and conductivity over frequency. Ψ_2 is the angle of the transmitting antenna between line-of-sight propagation and ground-reflected wave as seen in Figure 18. R_v is Fresnel reflection co-efficient, where *v* stands for vertical polarization.

$$\mathrm{w} = \frac{-j2kr_2u_2(1 - u^2cos^2\Psi_2)}{(1 - R_v)} \quad (7)$$

Equation 7. Function for w in equation 6 [28, p. 4].

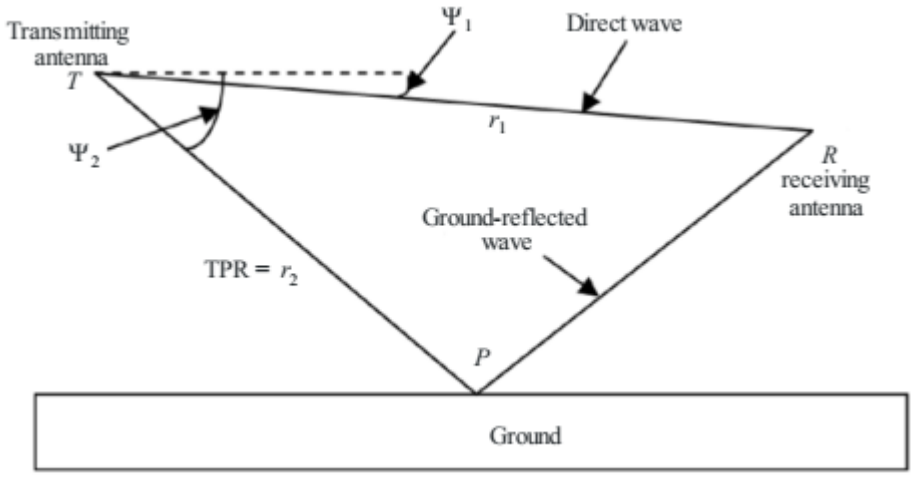

Figure 18. Propagation is where ground-reflected waves and direct waves reach the receiving antenna [28, p. 3]. The angle between these propagation methods from the transmitting antenna is used in Equation 7.

3.1.3 Inhomogeneous propagation model

Homogeneous propagation does not fit in all cases, as it is common to have an inhomogeneous surface, where the path varies over different conductivity

surfaces, such as water and land. Millington's model is used when the propagation path is over varying surface types and height variations [32, p. 133] [33, p. 6]. In this model the user needs to evaluate each segment of varying surface type and height individually.

The model divides the path into individual homogenous segments, requiring the knowledge of the propagation path and a knowledge or approximation of field strength, E in dB(μV/m), for each segment where there is variation in the surface type, this is illustrated in Figure 19. Each segment, S_n, is comprised of conductivity, σ_n, and permittivity, ε_n.

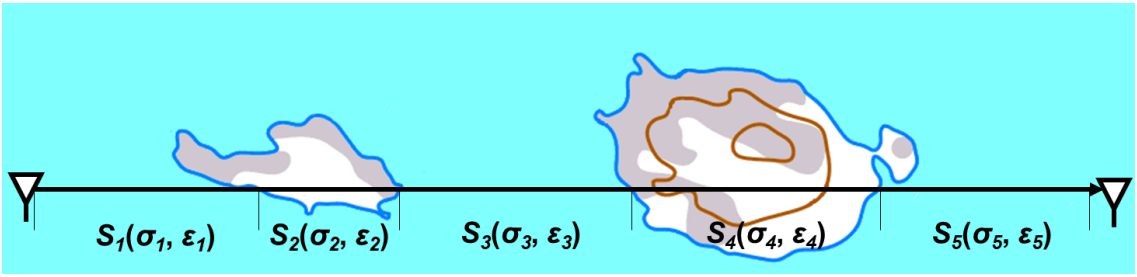

Figure 19. Millington's model. Wireless communication between stations with field strength changes five times. There should be two additional segments for elevation change in S_4, which are left out for easier readability.

The difference in path loss can be seen clearly when the propagation surface changes. In Figure 20, there is a three-segmented mixed path with sea-land-sea transition in four different frequencies. The surfaces are a 50 km long island at 75 km distance from the source and the rest is water. The total distance is 200 km, and the physical characteristics of the surfaces are for land σ = 0.003 S/m, ε = 15 and for water σ = 5 S/m, ε = 70. [34, pp. 4-5]

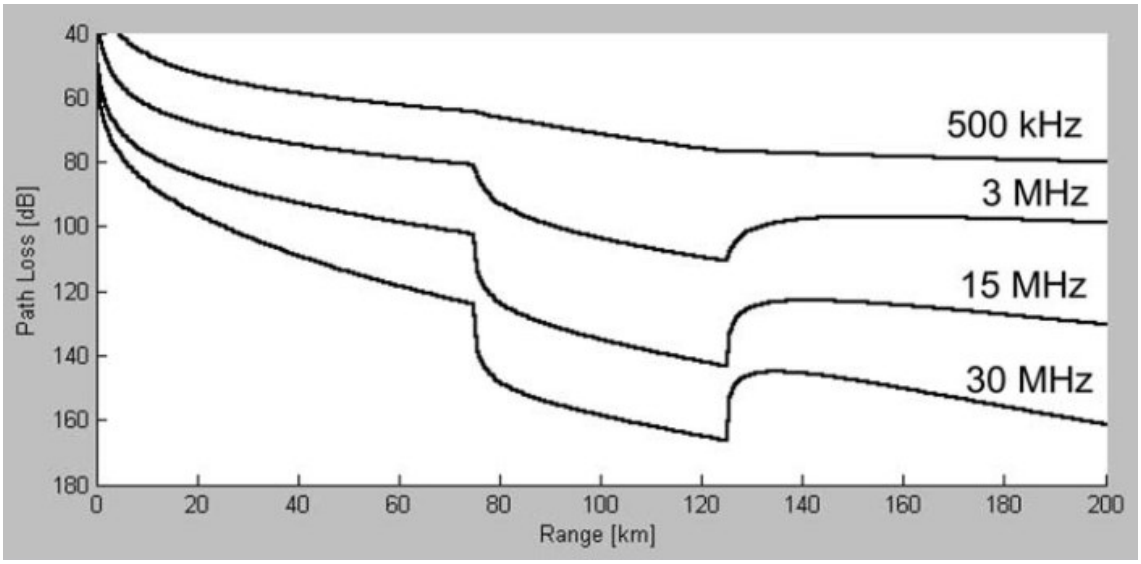

Figure 20. Millington's model's path loss on a mixed path: sea-land-sea [34, p. 5]. The dip in conductivity at 75 km, where the land begins, is noticeable on all frequencies except for 500 kHz, which is outside of the HF band.

From Figure 20 we can determine that HF is especially susceptible to changes in conductivity on the surface. However, at the low end of MF, at 500 kHz and below, the signal is not affected greatly by the change of conductivity, therefore the band has a longer potential range compared to HF in ground wave propagation.

Figure 20 contains another interesting phenomenon: a recovery effect. First, we see a dip when conductivity drops when the signal reaches land, but at the 125 km mark where propagation surface changes again to sea. There is a notable recovery in path loss value i.e., the increased signal strength of nearly 20 dB at 30 MHz. The recovery effect increases at higher frequencies, but at the same time the change of conductivity has a stronger effect. There is no additional value using higher frequencies.

3.1.4 Ground wave attenuation

As we have seen, attenuation is caused by path loss when the signal travels further away from the transmitter. Transmission distance in ground wave

propagation can be extended by increasing the transmission power, within limits.

Another form of attenuation is fading, which occurs when the signal has a phase change. Fading can be divided into small- and large-scale fading: small-scale is caused by multipath propagation and large-scale by large obstacles on the propagation path [35, p. 5].

While sea water has the highest conductivity it has an additional attenuating effect from waves, which are directly tied to sea state or specifically result of wave height. In 1970, Barrick modeled a system that proved that sea roughness would affect path loss up to 15 dB at 100 NM on 15 MHz frequency [36, p. 532]. In the same paper, he noted that on lower frequencies it may not have any effect or can have a positive effect on signal strength as seen in Figure 21.

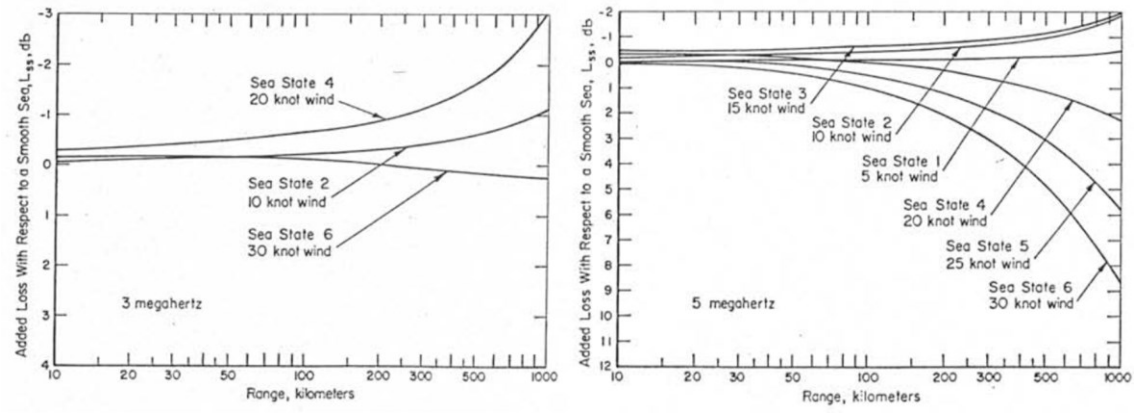

Figure 21. Barrick's model on the effect of sea roughness. Right 3 MHz and left 5 MHz, both have a conductivity of 4 S/m and permittivity of 80 [36, pp. 530-531].

A reflected wave may have an additive effect on the signal, when the sea state is calm or it could just as well be destructive, depending on the situation. At rougher sea states the effect increases, this is caused by absorption when the signal hits the wave and refracts towards an easier path, salty water. The incident angle would also be upwards, rather than forward when waves are higher because of the sharper angle of approach.

Terrain irregularities affect propagation, as proven by Millington's model, most often not for the better, but there are occasions where diffracted waves can increase the field strength. Vegetation on land is a common reason for attenuation, which varies by leaf type, moisture on a leaf, and amount of snow on a leaf. Urban and man-made objects, or surface clutter on the path are reducing the propagation distance. [37, pp. 12-13]

To model the path loss and field strength in complex environments such as the Finnish archipelago is dependent on too many variables for most of the propagation models for the ground wave. The closest reliable model would likely be TIREM, which relies on empirical data, accounting for buildings and terrain height variation to estimate path loss. TIREM is a proprietary model and not readily available to a consumer.

The Longley-Rice model, also known as ITM, can work within the upper limits of HF, from 20 MHz and up. ITM can account for topographical irregularities, atmospheric refractivity, and attenuation variables based on time, location, and situation to form a path loss estimation [38, p. 4].

The attenuation in the maritime environment will increase heavily in archipelago conditions compared to the open sea. Ground wave path loss is also affected by variations in conductivity and sea state.

Figure 22 shows a simulated path loss with ITM in Finnish archipelago conditions, The settings are median values fitted for both land and sea propagation as defined by ITU-R. This model is not perfectly fitted, but it gives an average idea. The reality may differ notably by time of year and weather conditions.

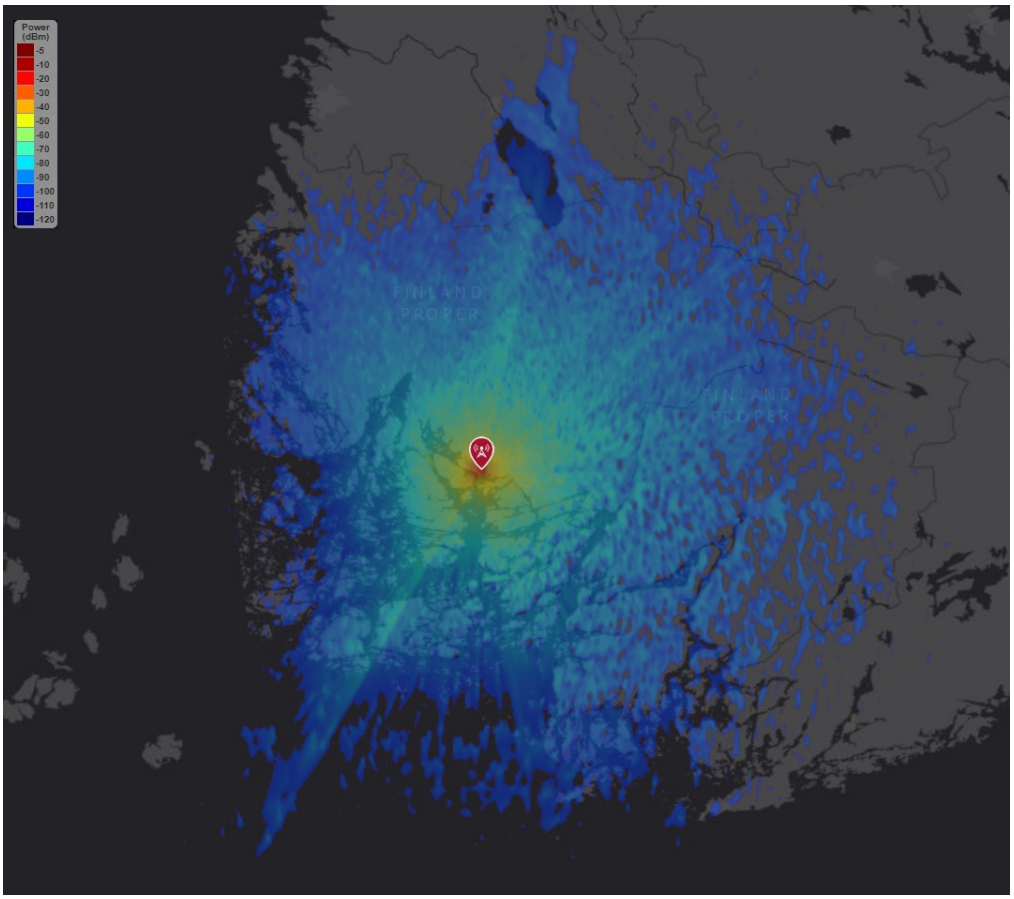

Figure 22. ITM simulation in the Finnish archipelago. Settings are conductivity 0.03 S/m, permittivity 40, omnidirectional vertical antenna at a height of 10 meters, and frequency of 20 MHz.

3.2 Skywave propagation

Skywave propagation has a desirable effect on RF communication for it can reach vast distances with proper preparation and antenna selection. It is based on an oblique or a near vertical incidence angle from an antenna to the ionosphere, which can refract the signal back to Earth if the frequency is within the optimal range [26, p. 2].

Successful link establishment and sufficient data throughput are heavily dependent on the correct parameter selection and even then, the ionospheric situation might suddenly change, severing the connection [26, p. 19].

For decades the success in skywave propagation has been reliant on the skill of the operator, which was a major reason for a decline in interest in HF communications.

As microprocessors became more common in the late 1970's, ALE, and later cognitive SDR, HF radios have become a standard [39, p. 55]. This has caused the return to the skywave propagation, as the human factor can be reduced or removed from the equation.

3.2.1 Ionosphere

The upper layers of the Earth's atmosphere form the ionosphere, which is ionized by the sun's radiation. As the sun is constantly in flux, so are these layers. UV and Gamma radiation emitted from the sun electrically charge these Earth's layers at heights between 80 to over 400 km [40, p. 12].

During the daytime our sun rips electrons from atoms in the ionosphere, causing it to ionize and stratify into distinct layers of varying ionization and height [41, p. 2]. As the solar radiation is blocked by Earth's nightside the free electrons recombine again with atoms restarting the process.

The ionosphere serves an important role in HF skywave communications, as it can refract signals of that specific frequency band back to Earth, permitting BLOS communications [42, p. 1-8]. The higher the electron density in the ionosphere is, the better it refracts the HF signal; meaning the higher the refracted frequency.

The ionosphere is divided into multiple layers that are subjected to periodic and irregular spatial and temporal changes [43, p. 39]. These are known as D-, E-, F_1-, and F_2-layers which vary in accordance with the day-night cycle, as depicted in Figure 23. The ionosphere can experience a sudden change in suitable frequency or even a complete loss in refracting capabilities.

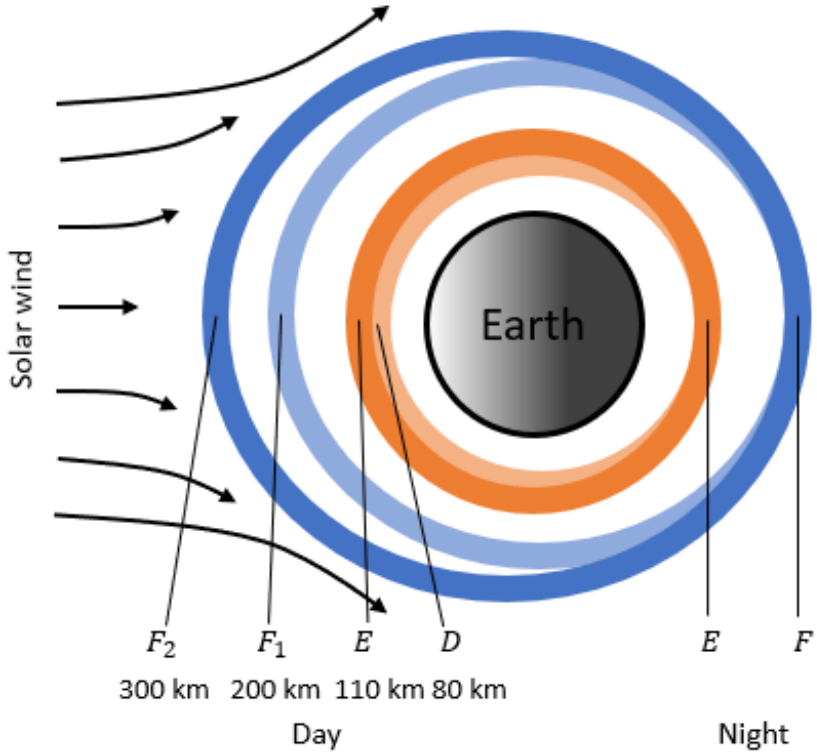

Figure 23. Ionospheric layers during the day-night cycle [39, p. 8].

The D-layer resides at an altitude of 50 to 90 km and is predominant only during the daytime when it is subjected to solar radiation [39, p. 9] [43, p. 40]. The notable effect of the D-layer is the absorption of RF signals by siphoning transmission energy to electrons [42, p. 1-23]. They begin to oscillate, if the frequency is above the LUF, the signal will continue on its path with a phase shift [42, p. 1-23].

The E-layer is situated between 90 to 140 km and remains during the nighttime, sporadic E-layer, E_s, appears in this layer [43, p. 42]. The E-layer may be used for an oblique propagation path of medium distance, around 200 km and up, at the lower range of the HF band of about 3 MHz and below [39, p. 11]. This layer is not as suitable for NVIS propagation because of reduced coverage caused by a lower altitude of the E-layer.

The F-layer is divided into F_1 and F_2 during the day, which merge during the night as one, at an altitude of 140 to 600 km, and on occasion reaching the

upper limits of the ionosphere [43, p. 42]. Electrons in F-layers are the ones that are most affected by ionization from solar activity, therefore they are the main layers used in skywave communications.

The layers E, F_1, and F_2 each have their own critical frequency denoted as foE, foF_1, and foF_2. These are directly related to the maximum density of electrons in these layers, as shown in Figure 24, where orange depicts the electron density and blue is the area of frequency reflected by the layer [42, p. 1-10]. Everything below f_{min} is absorbed and anything above foF_2 penetrates the ionosphere.

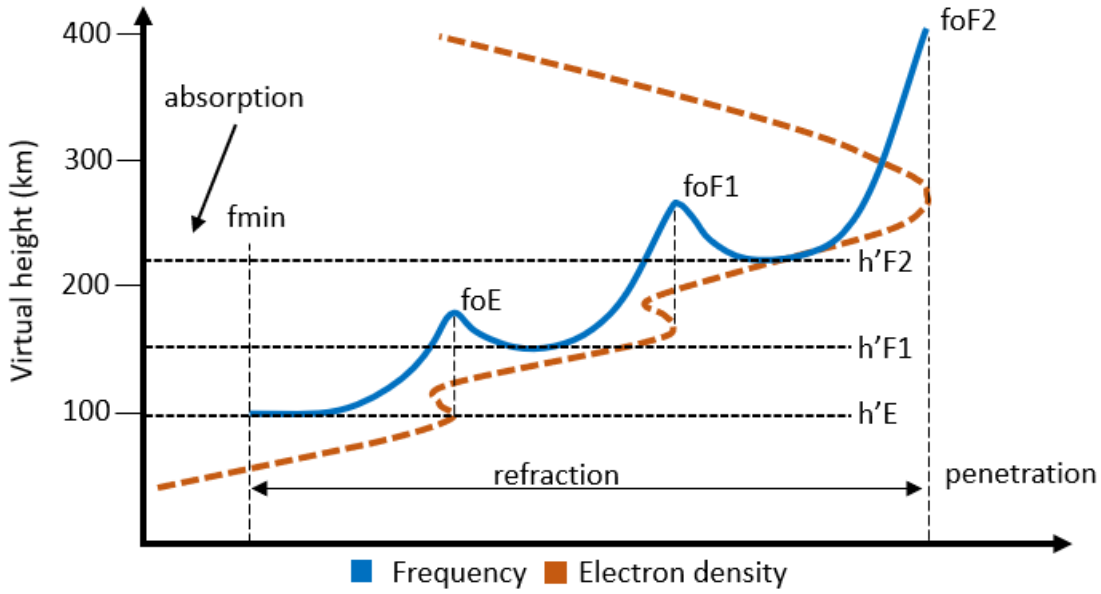

Figure 24. Relationship between the electron density and ionospheric critical frequency [42, p. 1-11].

Sporadic E, E_s, is a randomly forming unusually dense ionized electron cloud in the E-layer, in an area less than 1 km in depth and 70 to 150 km^2 [44, p. 27]. Formation of a sporadic E can prevent a signal from being transmitted to the F_2-layer and prevent communication to the receiver as the hop distance changes.

While sporadic E happens irregularly, they usually dissipate within a few hours and drift at a velocity of several hundred kilometers per hour, as such they are more of a nuisance and rarely can be used for benefit [44, p. 27]. In the

Northern Hemisphere, they appear in summertime from May to August and in winter in early December, often accompanying aurora borealis [45, pp. 23-29].

Single hop on at a 0-degree angle of elevation antenna can reach up to 2000 km when the E-layer is at 100 km and the F-layer at 300 km maximum hop distance is 4000 km, in southern latitudes [42, p. 2-8]. In the northern latitudes, where the ionospheric conditions are worse, the distances might not be comparable.

The ionosphere is an anisotropic and inhomogeneous medium for RF signals to propagate in, this can cause unexpected situations, such as one-way communication [32, pp. 186-187]. The ionosphere causes changes in signal polarization, but in return the signal is elliptically polarized, permitting the use of both vertically and horizontally polarized antennas for reception.

3.2.2 Antenna

Skywave propagation is heavily influenced by the antenna choice and proper antenna selection can be one of the defining factors in establishing an HF link. Different kinds of antennas are optimized for the task they are built for, they all have pros and cons.

An important feature in HF antenna selection is the skip zone, formed between where the ground wave ends and the skywave begins. The skip zone has no connectivity, as the transmitted signal is not present. The goal of antenna and frequency selection is to relocate, reduce, or remove the skip zone.

All antennas have a radiation pattern to direct the transmission to the desired direction [4, p. 20]. This increases the antenna gain by focusing the transmission towards the receiver, or in a case where both transmitter and receiver are moving, the antennas are likely omnidirectional.

The directionality also causes limitations: transmission’s take-off angle cannot exceed the confines of radiation pattern and at reception, too high incidence

angle will attenuate the transmission, Figure 25. The antenna begins to lose its efficiency at HPBW in the main lobe, or -3 dB from maximum gain, after that antenna can be deemed unsuitable for the task [4, p. 26].

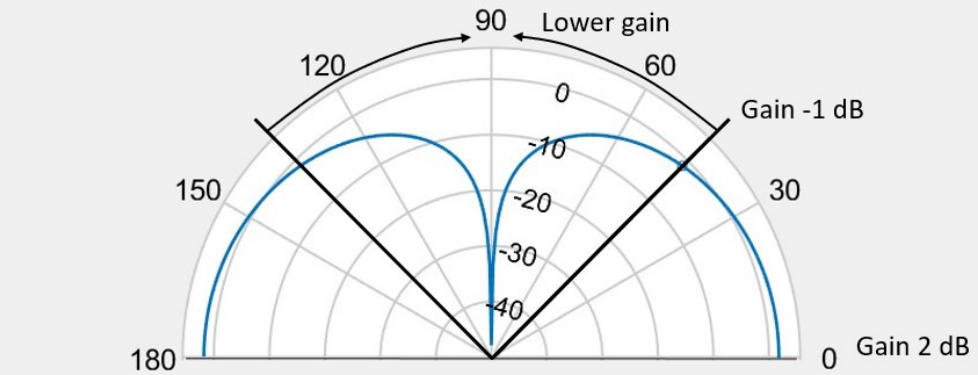

Figure 25. 7-meter vertical monopole antenna far-field at 8 MHz. The blue line shows the radiation pattern. The black line indicates HPBW at 45 degrees from ground level.

A 7-meter monopole is a common selection on a ship, as it is easy to mount and can handle strong winds due to a small wind surface. It is also well suited for both ground wave and skywave propagation. However, as it is evident in Figure 25 the transmission angle is an issue for close-range skywave as it needs a more vertical angle to propagate.

Transmissions received at an oblique angle from the ionosphere is known as the critical angle of incidence, φ_0, and it can be calculated with Equation 8. Where θ is the acute angle between two points on the ground, h' is the virtual height and R represents the radius of the Earth. Figure 26 shows these values with symmetrical and spherical ionosphere above the Earth.

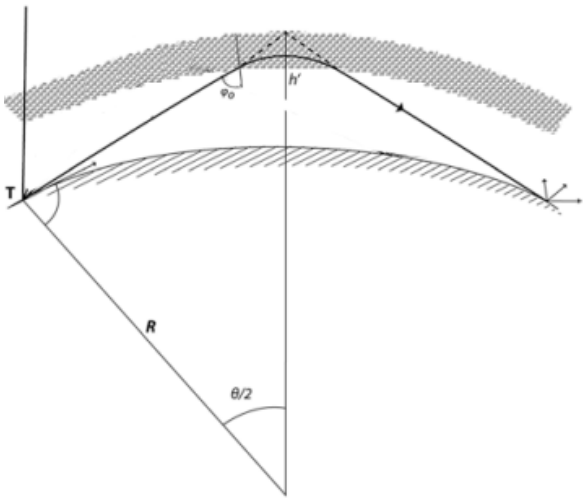

Figure 26. Critical angle of incident for skywave propagation [43, p. 186].

$$\varphi_0 = \tan^{-1} \frac{\sin\frac{\theta}{2}}{1 + \frac{h'}{R} - \cos\frac{\theta}{2}} \quad (8)$$

Equation 8. Critical angle of incidence [43, p. 186].

Using the critical angle of incidence, the MUF can be calculated with Equation 9. Critical frequency, f_o, is the highest possible frequency at a 90-degree angle from the Earth that is capable of refracting from the chosen layer at the current ionospheric conditions.

$$MUF = f_o \sec \varphi_0 = \frac{f_o}{\cos \varphi_0} \quad (9)$$

Equation 9. Maximum usable frequency, also known as the secant law [43, p. 187].

NVIS antennas are better suited for more vertical angle transmissions than oblique with a smaller to no skip zone but are ill-suited to ground wave propagation. Due to the more vertical incidence angle at the ionosphere, they need a lower frequency than the oblique angle and less transmission power due to a shorter distance in the D-layer [39, p. 12].

Because the angle of NVIS is vertical, instead of oblique, the used frequency matches that of the critical frequency and is therefore directly applicable to the value that an ionogram provides [39, p. 10] [42, p. 1-8]. Suitable frequencies may range from 4 to 8 MHz during the day and 2 to 4 MHz during the night [46, p. 10].

3.2.3 Solar and Atmospheric Effects

HF communication is affected by changes in solar activity. The most critical event in the photosphere, which plays a primary part in all other solar activity affecting Earth's ionosphere, is the sunspots [43, p. 15].

Sunspots are cooler than normal formations in a small region, appearing as dark spots on the Sun's surface [41, p. 2]. These spots are tied to strong magnetic fields, which prevent the transfer of gases from within the Sun to the photosphere. The density of these spots is tied to an 8–14-year cycle, commonly known as the 11-year solar cycle, Figure 27 [43, pp. 15-16].

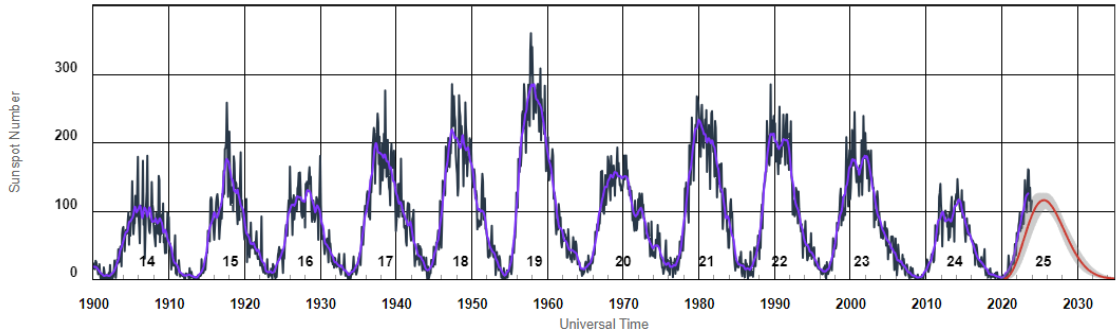

Figure 27. The observed solar cycles from 1900 to 2023, the current solar cycle is the 25th [47].

A solar flare is a sudden and violent localized release of energy from the Sun, commonly associated with a growing or magnetically complex group of sunspots [42, p. 3-13].

When a solar flare erupts it is accompanied by emissions across the entire spectrum, including radio, UV, and X-ray frequencies. In addition, the solar flare produces large quantities of Gamma- and X-rays, protons and electrons in superheated plasma [43, p. 18]. Table 2 shows common emissions from the Sun, describing effects that can appear quickly and have long aftereffects.

Table 2. Types of solar emissions [43, p. 162].

Solar emission	Time of transit to Earth	Terrestrial consequences
X-rays	8.3 min	Sudden ionospheric disturbance
Protons	A few hours	Solar proton effect
Low energy plasma	1-2 days	Geomagnetic storms and aurora

The X-ray emissions from a solar flare are the initial effector, but the severity of them is dependent on the magnitude of eruption from the Sun. The magnitude of X-ray flux is denoted as A, B, C, M, and X-class, where M and X-class are considered important as they cause longer SIDs, but are infrequent in comparison to A, B, and C [42, p. 3-14].

The immediate effects of X-rays on HF can cause signal fading, bursts of noise, buzzing, and potentially loss of connection [41, p. 5]. Depending on the intensity of the X-ray emission, the SID can last from a few minutes up to many hours with a median being 15 to 90 minutes varying by the classification [48, p. 7].

SID affects lower frequency HF connectivity stronger than the higher, as the D-layer gets more ionized than normally. It is also slower to recover from the effects of the solar flare, as seen in Figure 28. This can be compared to Figure 24, where f_o and D, F_1, and F_2-layer ionization are visible, and the effect of the solar flare extends the D-layer to a higher frequency and increases absorption [42, pp. 3-22-23].

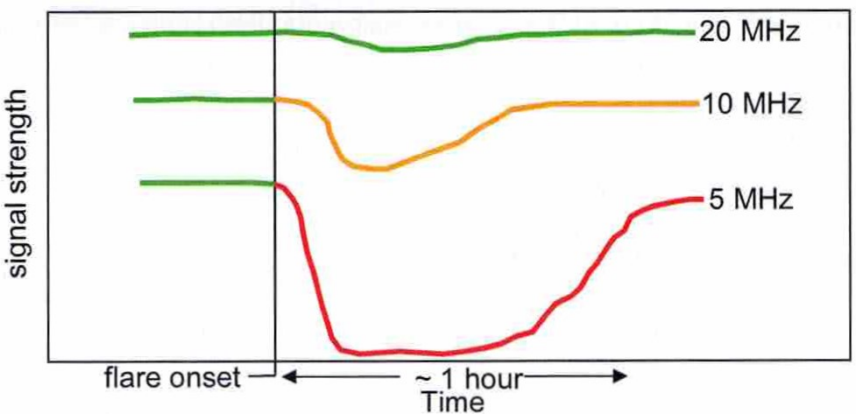

Figure 28. Example of an effect from a solar flare on HF communications at frequencies 5, 10, and 20 MHz, which becomes less severe at higher frequencies [42, p. 3-23].

Large solar flares or CME shockwaves can accelerate protons, known as a solar particle event, at collision with the Earth's magnetic field [42, p. 3-25]. This guides these protons to the polar regions, resulting in a strongly ionized D-layer and strong absorption [42, p. 3-25]. This event is called polar cap absorption, and it can last from several hours to a few days [43, p. 163]. Absorption will be strongest on the dayside but will make the D-layer appear on the nightside as well.

Events where the Earth's magnetic field is disturbed by solar winds, the fluctuations of strength and direction are called geomagnetic storms, directly affecting Earth's magnetic field [42, p. 3-27]. Plasma in the solar wind is highly ionized and electrically conductive.

This can have a two-sided effect: negative or positive. The negative effect lowers the F-layer electron density to levels where HF communication can become limited or impossible on higher frequencies. The positive effect has no hindering effects on HF but can instead enhance individual layers. [42, p. 3-31] [48, pp. 4, 164]

Geomagnetic storms are associated with CMEs and an aurora, these are a common indicator for a storm. Negative storm effects first appear on the nightside auroral and sub-auroral zones [48, p. 4]. A storm affects the HF communication, as visible in Figure 29, by reducing the usable HF band. It can also affect satellite communication and, if severe enough, power grids.

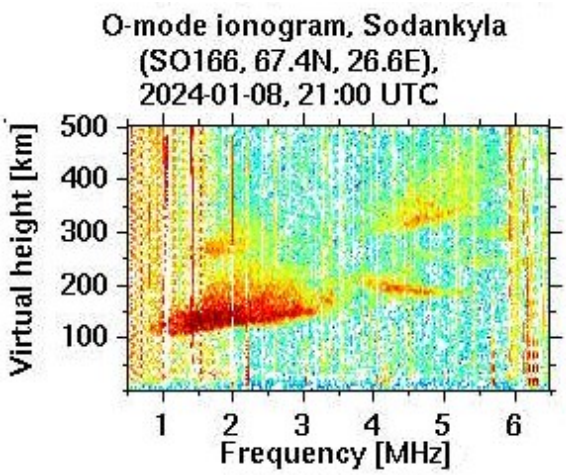

Figure 29. Effect of an aurora borealis as seen on an ionogram (zoomed) [49].

3.2.4 Skywave attenuation

The ionosphere is not an ideal medium, as signals propagating through are subjected to fading and Doppler spread on both time and frequency. Rapidly occurring changes in the ionosphere, be it solar, diurnal, or seasonal, cause faster fluctuations and fading in the skywave channel, increasing the unreliability of HF communications. [39, p. 12]

D-layer has a negative effect as it absorbs the signal each time it passes through the layer or prevents communications entirely, as described earlier. During the night as the D-layer is absent, the attenuation is reduced, and lower frequencies are applicable. Sporadic E-layer can change the propagation path suddenly, just to vanish as quickly as it appeared.

The total ionospheric absorption can be presented with Equation 10. Where κ is an imaginary part of the complex propagation function k and ds is the distance of the propagation path. The complex function is defined as $k=2\pi fn/c$, and can be broken down into signal frequency, f, complex index of refraction, n, and speed of light, c.

$$L_a = -8.68 \int \kappa \, ds \tag{10}$$

Equation 10. Total ionospheric absorption [50, p. 767].

While single hop is preferred in HF communications, it is occasionally required that over long distances multi-hop path to be used. Each hop increases the attenuation of the signal, when passing through each layer and when reflected off the ground. The signal strength suffers especially from ground reflection, as some of the energy is scattered instead of reflected. The multi-hop path can have a path loss exceeding 100 dB [39, p. 11].

In HF communications frequency shift happens because the average height of the refracting ionospheric layer may vary over time or by point of refraction, which means each multipath has a Doppler spread [51, p. 1]. This is called fading, and it is caused when multipath propagation signals are out of phase from each other and have a destructive effect, reducing the amplitude of the signal [39, pp. 12-13].

In Table 3 are reference values for time delay and Doppler spread in three geomagnetic latitudes tied to geographic regions. Here is evident the degraded ionospheric conditions in the northern hemisphere.

Table 3. Doppler spread and time delay by geomagnetic latitudes [51, pp. 10-11] [52, p. 8].

	High latitude 90˚ > λ > 60˚		Mid latitude 60˚ > λ > 20˚		Low latitude 0˚ > λ > 20˚	
	Delay	Doppler	Delay	Doppler	Delay	Doppler
Quiet	1 ms	0.5 Hz	0.5 ms	0.1 Hz	0.5 ms	0.5 Hz
Moderate	3 ms	10 Hz	2 ms	1 Hz	2 ms	1.5 Hz
Disturbed	7 ms	30 Hz	7 ms	1 Hz	6 ms	10 Hz

Even with all this considered the path loss for skywaves is notably less than for ground waves, but the ionosphere's potential for sudden changes makes it an unpredictable propagation path. Both means of propagation are valid to an extent and complement each other's.

3.3 Noise and interference in HF spectrum

In all RF communications noise is the determining factor if the information in the signal can be understood [26, p. 65]. Noise is a signal that can be received, but it is a byproduct of environmental effects and serves only to limit the reception threshold. Noise floor is a term used to indicate the baseline strength of a noise at any given location and frequency.

If the transmitted signal has too-low power at the receiver in relation to the noise, the message cannot be distinguished from the noise. SNR is a comparison of the strength of the desired signal to the noise, Figure 30. Required SNR varies depending on the complexity of the transmitted signal.

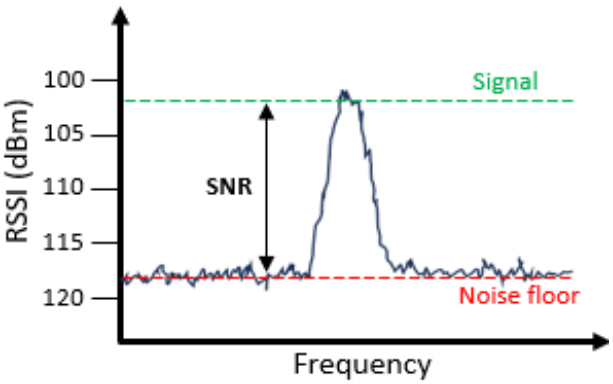

Figure 30. SNR is a difference between desired signal and noise floor.

ITU defined noise factor in an HF channel, Equation 11, when the receiver is free of spurious signals. Where f_a is the external noise factor, f_c is the noise factor for antenna circuit losses, l_c is the antenna circuit loss, l_t is transmission line loss and f_r is the internal noise factor for the receiver. Total noise is a sum of transmitter, channel, and receiver noise.

$$f = f_a + (f_c - 1) + l_c(f_t - 1) + l_c l_t(f_r - 1) \tag{11}$$

Equation 11. Noise factor [18, p. 4].

A large part of the noise in HF channel is impulse or burst noise, which causes unpredictable, short-lived, and rapid fluctuation in the noise floor [39, p. 14]. The amount of noise is also tied to the size of bandwidth used, larger bandwidth results in increased noise and vice versa [54, p. 499].

Noise can be divided into internal and external noise. Internal noise is caused by mismatch loss, the antenna radiation efficiency or directivity of the antenna, or a combination of these [53, pp. 3-4]. Internal noise can be reduced by a well-matched radio system and antenna suitable to the frequency band.

External noise appears in an RF channel and can be divided into three major sources, atmospheric, cosmic, and man-made, which are so powerful that they usually overwhelm the internal noise of the receiver [39, pp. 13-14]. Noise is more severe on the lower band of HF; mitigation happens at 10 MHz and higher HF frequencies are quieter [18, pp. 6-7].

A sporadic electromagnetic field is created near a lightning strike, which is the most significant natural cause of noise in an HF band at frequencies 20 MHz and below [26, p. 66] [32, p. 250]. The lower the frequency, the higher the amplitude of the noise from these events.

Another natural noise source in a propagation path is cosmic background noise. This source’s effect on HF is highly situational to the location and at any given time.

Man-made noise is the largest contributor to external noise, in it can be defined as thermal noise and interference caused by other users on the same or nearby frequency. As the HF band is narrow and suitable frequencies at any given time are limited to an even narrower band, the likelihood of interference from other users is high.

Thermal noise is caused by every conductive material with a temperature above absolute zero, including other antennas, electronic machinery, power lines, and industrial machinery [18, p. 3].

A common way to model noise in an HF channel is AWGN, it does not calculate fading, interference, or dispersion, which are present in a real channel [39, p. 14]. The real channel is tied to a location and measurements may vary on a diurnal and seasonal scale and a longer annual basis.

The Watterson model is an expansion to AWGN, which accounts for multipath and fading, simulating propagation in the ionosphere [55, pp. 1-3]. The model is divided into multiple taps simulating individual multipaths, each having their Gaussian randomizer for frequency shift, power gain, and standard deviation.

4 Defining ISB tactical data link performance requirements

The system shall use PSK and QAM modulations with convolutional encoding, punctured to a code rate of ¾, to convey transmitted data on two individual 3 kHz channels with data interleaving [14, p. 109]. Access management will be handled with TDMA. The modulation scheme will be identical for both channels, while the information is unique.

It would be possible to expand the bandwidth of a single sideband up to 48 kHz, but that would be outside of most HF radio system's capabilities [14, p. 141]. As most of the HF radios are still narrowband, the 3 kHz bandwidth will suffice. This will support wideband radios in the future by expanding the number of 3 kHz channels within each sideband.

A transmitted data frame consists of a preamble, data blocks, and mini-probes. The preamble is divided into two parts; the first part is for radio and modem AGC. The second part of the preamble is used to handle synchronization and Doppler offset to the receiver, it also provides information on interleaving settings and uses a modulation scheme. [14, p. 120]

Data blocks are followed by mini-probes and periodically by shorter reinserted preambles. Both help the receiver to maintain synchronization, help combat

against Doppler shift, and inform the receiver of the current interleaving sequence [14, pp. 123-125].

A modern tactical data link system with the ability to change frequency and waveform settings needs a unit that manages these functions. LINK 22 fits HF capable data link description and identifies this management unit as the Network Management Unit, which is responsible for individual radio networks within a Super Network [19, pp. 1-6, 1-26].

4.1 Digital Modulation Schemes

While in RF communication the channel is always analog, with the use of modems digital information may be encoded to an analog channel and converted back to digital at the receiver [39, p. 24]. Digital modulation provides numerous benefits over analog, such as efficient use of spectrum, easier encryption, error correction methods, better spectral efficiency, and encoding [56, p. 126]. Combining the digital modulation with analog signals and encoding we get a waveform.

Digital modulation is depicted in a constellation diagram for easier readability and better detection of suitability by varying levels of SNR. A higher modulation order means more transmitted symbols and a faster data rate but also reduces the robustness of the signal [3, p. 197].

Decision regions are the zones in the constellation figure, which determine the symbol value extracted from the signal [56, pp. 134-136]. Gray mapping is used to limit the effects of SNR, where there is only a single number changed between symbols.

Figure 31 depicts constellations and signals of 8PSK and 16QAM, while not all decision regions are visible, it is evident that in the denser symbol pattern, there is less room for error and thus higher potential for an error bit. Worse conditions in the propagation path require a lower modulation order.

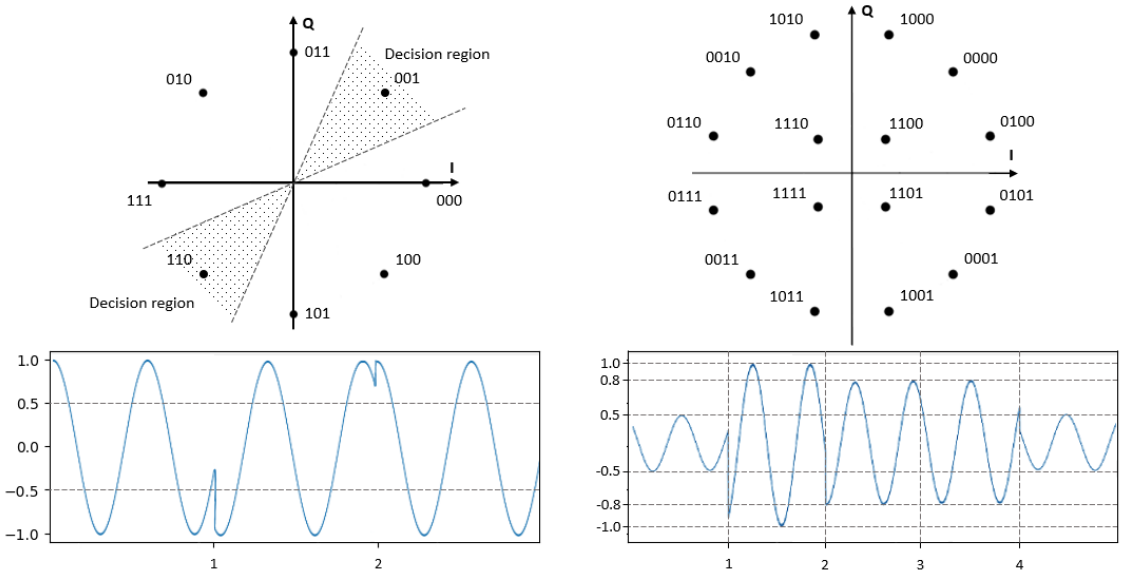

Figure 31. An 8PSK constellation and signal example on the left and the same for a 16QAM on the right, as defined in MIL-STD-188-110D [14, pp. 147-148].

Figure 32 shows the effect that noise and Doppler shift in the propagation channel have on the received signal. Red dots indicate the received symbols and black dots the symbol location. In the left example, the noise spreads the reception, an error does not occur if the received symbol remains within the decision region. In the right example, the Doppler shift rotates the received symbols off the center by the magnitude of the shift.

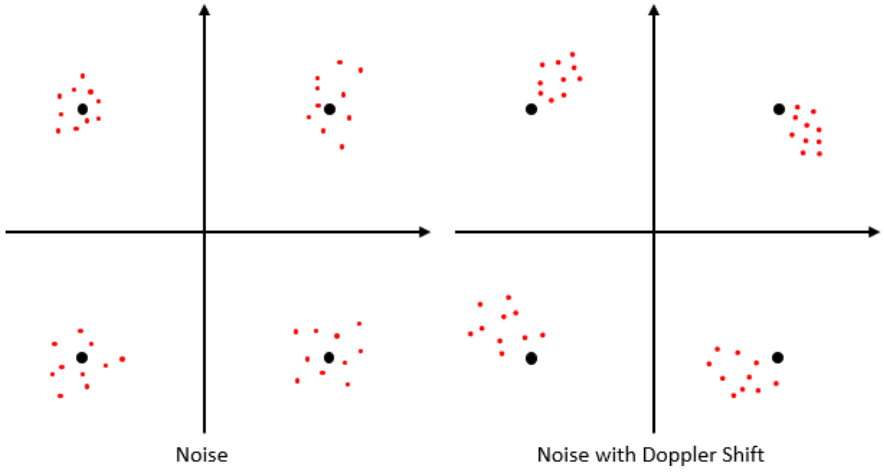

Figure 32. Effects of the noise and Doppler shift to the received symbols.

PSK is reliant on phase shifting as a means of detecting the symbols. The higher the modulation order, the higher the peak amplitude is required to accommodate the detection, making PSK power-inefficient above 8PSK [39, p. 190].

In QAM the symbols are retrieved from changes in amplitude and phase, making it spectrally more efficient than PSK, it is an excellent modulation for a higher modulation order [56, p. 148]. However, it is important to recognize the level of noise and fading in the propagation path.

4.2 Bit error rate and encoding

BER is a term for the probability of how many incorrect bits are received, causing degradation in transmission performance. BER occurs when a symbol is received incorrectly due to a sudden burst or constant signal degradation from noise, as depicted in Figure 33 [54, p. 682].

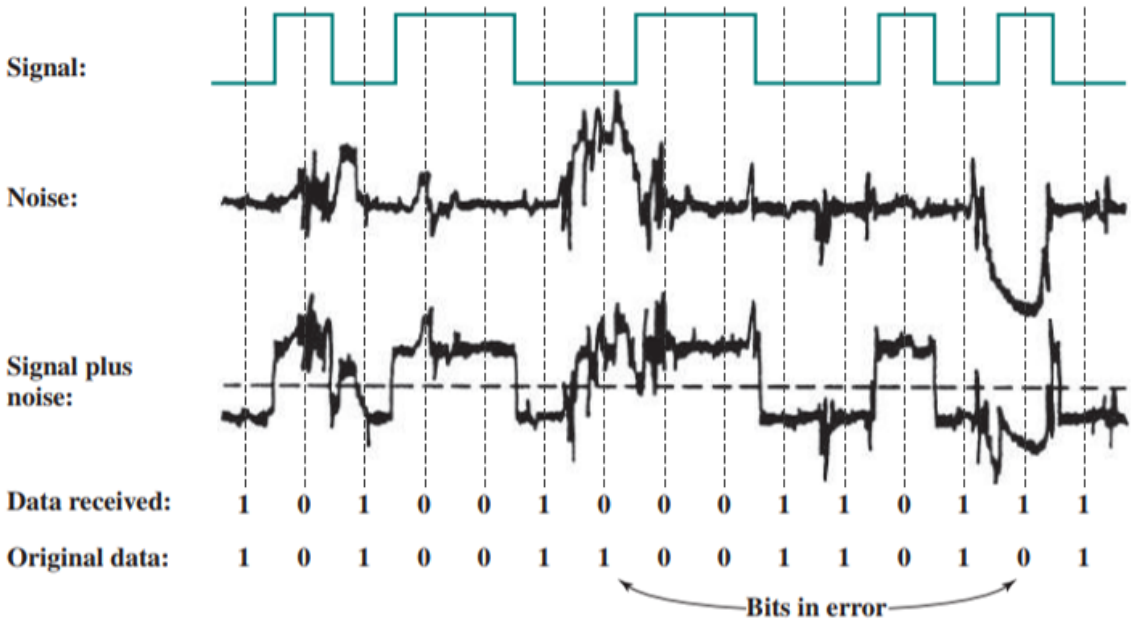

Figure 33. Effect of noise when receiving digital information [3, p. 122].

The probability of a BER is closely related to E_b/N_0, which is the quotient of power of the transmitted bit, E_b, to noise power density per hertz, N_0, depicted in Equation 12. Where S is the signal power, R is the data rate, k is the Boltzmann constant, and T is the noise temperature in Kelvin.

$$\left(\frac{E_b}{N_0}\right)_{dB} = S_{dBW} - 10\log R - 10\log k - 10\log T \tag{12}$$

Equation 12. The ratio of signal energy per bit to power density of the noise per hertz [3, p. 126].

BER is a valuable tool for estimating a suitable modulation order when combined with knowledge of the electromagnetic environment. The BER of digital information increases, the worse the SNR gets. The higher the modulation order becomes, the better the SNR values must be, as can be seen from Figure 34. The quality of the connection determines the maximum throughput from the digital modulation.

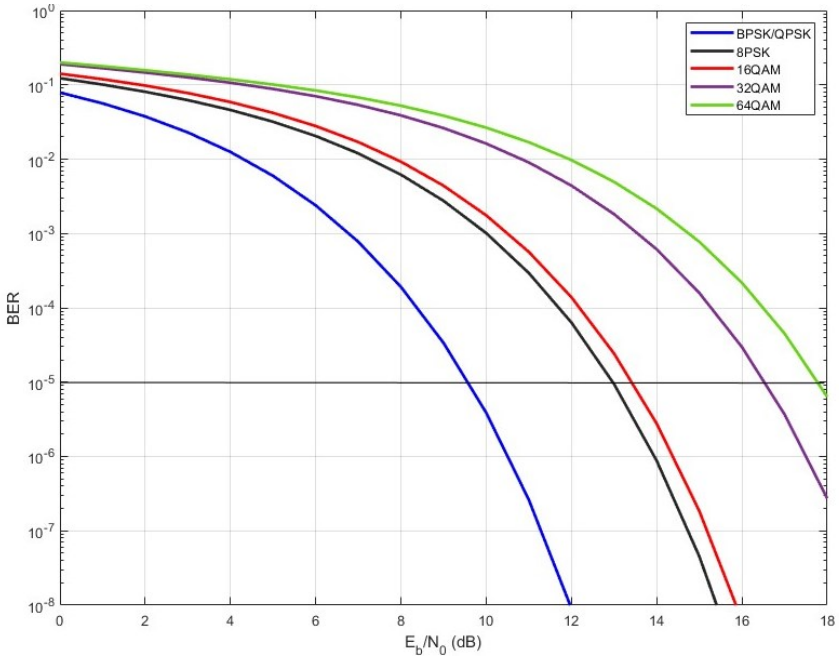

Figure 34. On the left a theoretical BER to E_b/N_0 for the evaluated waveforms in an AWGN channel. BPSK and QPSK have the same performance in AWGN when properly mapped to the bits.

When looking at Figure 34, QPSK seems an obvious choice over BPSK, as you gain better spectral efficiency. Still, there are benefits in using BPSK in situations, where jamming or an exceptionally poor propagation path occurs. The decision region of BPSK is double compared to QPSK and it is less affected by severe Doppler shift [3, p. 190].

The requirement for ISB data transmissions on a fixed frequency must achieve BER $1x10^{-5}$, when using maximum interleaving length [14, p. 263]. ISB and SSB can have the same SNR requirements to achieve this level of BER. However, in an equivalent channel, ISB always has worse SNR, as it loses minimum of 3 dB due to the modulation inefficiency.

Encoding can also be used to improve the signal against fluctuation in SNR, which nominally reduces the useful bits by introducing a parity bit to provide forward error correction. Encoding requires sacrificing some of the data bits to create redundant bits, which reduces the throughput. A code rate of ½ requires twice the capacity, in bandwidth or modulation order, compared to the uncoded transmission. A code rate of ¾ would require 33% of the data rate. [3, pp. 227-229]

The benefit from this drop in throughput is improved robustness of the signal. A situation where there is an unusable level of SNR for an uncoded signal, the connection may still be achieved a coded signal. The trade-off must be calculated, and the gain needs to overcome the throughput loss of coding.

Figure 35 shows theoretical estimations for QPSK and 64QAM with Reed-Solomon and Convolutional coding, these are coding gains in dB at BER $1x10^{-5}$. Depending on the encoding method, the coding gain can reach over 3 dB with Convolutional code. Gained benefits are notable, especially in a disturbed propagation path.

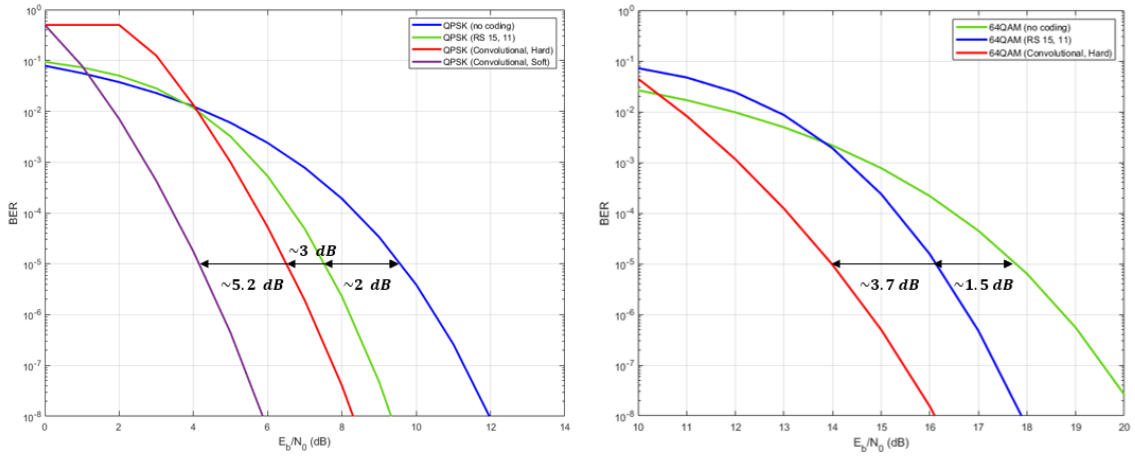

Figure 35. Theoretical QPSK and 64QAM in AWGN channel with Reed-Solomon and Convolutional channel coding.

Signal encoding is suited to situations where the fluctuations in SNR are short, in an ionospheric channel this is often not the case. The SNR can vary rapidly and intensively, especially in frequencies below 10 MHz.

Interleaving can alleviate this problem, as it can spread the error to smaller blocks all around the message, reducing the effect on individual parts of the message. The length of the interleaving must match the level of disturbance in the channel; a more disturbed channel requires a longer interleaving. [39, p. 25]

In Table 4 are the MIL-STD-188-110D defined data rates and SNR requirements for the modulations evaluated for both SSB and ISB transmission. The SNR values for both AWGN and ITU-R poor channel conditions are defined by BER requirement, and the interleaving period is set to maximum [14, p. 263]. ITU-R Poor channel conditions consist of two independent Rayleigh fading paths with a 2 ms delay and a frequency spread of 1 Hz [57, p. 2].

Table 4. SNR levels required by each digital modulation scheme for BER $1x10^{-5}$, when interleaving is set to Very Long [14, pp. 111, 134, 259, 263].

Digital modulation	Single sideband transmission			Independent sideband transmission		
	Data rate (bps)	AWGN channel	ITU-R poor channel	Data rate (bps)	AWGN channel	ITU-R poor channel
QPSK	3200	9	14	6400	-	-
8PSK	4800	13	19	9600	13	21
16QAM	6400	16	23	12800	16	25
32QAM	8000	19	27	16000	19	29
64QAM	9600	21	31	19200	21	34

To be noted about Table 4, is that ISB has no difference in AWGN channel compared to the SSB, and for ITU-R poor channel has only 2 dB difference, except for 64QAM. This is peculiar, as the mathematical best-case signal efficiency of double sideband transmission compared to single sideband is 50%, which translates to -3 dB, not to -2 dB.

The reason for this disparity is not elaborated in the document. It may be an indication of some inherent correction or gain happening due to the two preambles instead of a single preamble from two channels. Other options are that it is an estimation for the difference, or it is based on test results.

5 Measurements

The measurements are evaluated by SNR levels. Comparing SNR to reference ISB values and to mathematically calculated -3 dB inefficiency loss against SSB values, both set by MIL-STD-188-110D. Usable modulations are determined by meeting SNR requirements for 75% of the estimated connectivity time.

The reception was determined by RSSI values, as displayed by the radio. This was also used to measure the noise floor and identify the peak strength of burst noises. Connectivity was determined by the reception of the message,

regardless of the quality. In cases when there was no reception the RSSI has been ignored.

Measurements were done by using Rohde & Schwarz XK2100L radios, with a measured RMS power of 44 W. The distance between the transmitter and receiver was approximately 800 km. The first test was done in November and the second in February.

The transmitter antenna had a gain of approximately 1.9 dBi and the receiver antenna had a gain of approximately 2.4 dBi, both with 30-degree take-off angle. It should be noted that the gain of both antennas is superior to a standard ship-mounted monopole antenna at the same take-off angle.

Tests were performed with 3 kHz QPSK SSB at an 8 MHz fixed frequency. SSB was selected due to the transmitter's limitations. The fixed frequency was maintained to highlight the rapid changes in the ionosphere and how it affects the propagation path.

The frequency was selected based on calculated suitability from previous weeks' real-time ionogram data and estimations from VOACAP. It is a free HF propagation prediction software, which bases the predictions on empirical data.

The data is presented in dBm, as a dimensional unit it is a sufficient scale to compare the SNR for BER requirements for each modulation investigated. Upon reception the dBm is shown as a negative value, this is a normal means of presentation for signal reception.

Data collected between November 22nd and 24th, 2023, was collected at 30-minute intervals. There is a notable variation in the strength of the received signal, fluctuating between -52 dBm and -74 dBm, with a peak signal strength of -47 dBm. The noise floor and peak burst noise were recorded as well. Figure 36 depicts the collected data from the first test, where green indicates received signal strength, red the noise floor and a dotted red line indicates the peak burst noise.

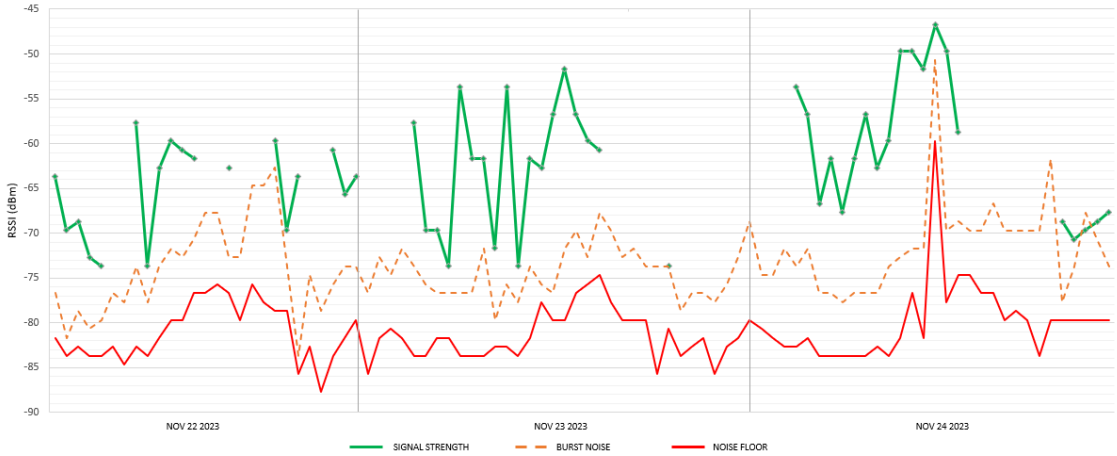

Figure 36. RSSI of QPSK SSB waveform, noise floor, and recorded burst noise levels from the first test conducted during November 2023.

Fading occurred on multiple occasions during the measurements done in November 2023 and RSSI had strong fluctuation. On November 23rd, 2023, two M-class solar flares occurred and another one on the 24th [58]. This and the resulting Aurora Borealis on the 24th are the likely reasons why there were large gaps in the connectivity. The ionospheric data recorded during this period is presented in Appendix 1.

During the 24th at 14:30 UTC an unusually high level of noise floor and burst noise were recorded. This may have been caused by another transmitter or thermal noise caused by an industry nearby the receiver. This spike should be considered an isolated occurrence, but it will be factored into the results regardless.

The SNR values are compared to the PSK and QAM modulation SNR to BER requirements depicted in Table 4. While Table 4 does not state the value for ISB QPSK, it can be estimated by comparing the other values, resulting in 9 dB for AWGN and 12 dB for ITU-R.

In Figure 37 the black solid line indicates the measured SNR, with measured values visible. The dotted black straight lines are for the AWGN channel, and

the red lines are for ITU-R poor channel value. Anything below the SNR line is usable, in theoretical channels, at the moment of measurement.

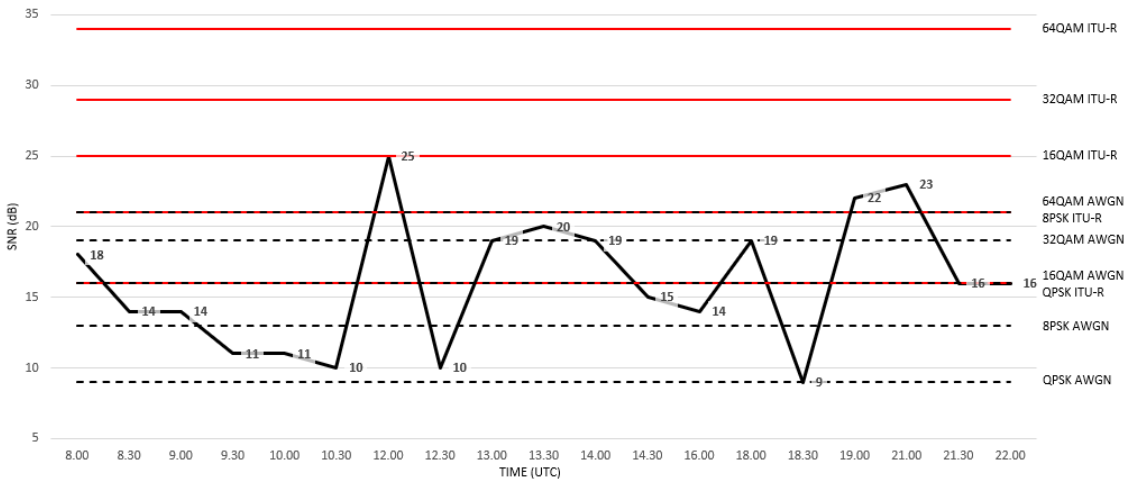

Figure 37. Measured SNR on November 22nd compared to the SNR requirements of each waveform, as defined in MIL-STD-118-110D.

Table 5 shows the average percentage of time that each ISB waveform would have been usable during the November 22nd test. Table 5 shows two options, one which follows the requirement set to ISB by MIL-STD-188-110D and another which adheres to SSB values stated in Appendix C but accounts for the mathematical efficiency drop of -3 dB when using ISB.

Table 5. Potential usable ISB waveforms during the November 22nd test, values for both MIL-STD-188-110D and optimally calculated half efficiency.

Waveform	MIL-STD-188-110D		Calculated (-3 dB)	
	AWGN	ITU-R	AWGN	ITU-R
QPSK	100 %	55 %	75 %	45 %
8PSK	75 %	20 %	55 %	20 %
16QAM	55 %	5 %	40 %	0 %
32QAM	40 %	0 %	20 %	0 %
64QAM	20 %	0 %	5 %	0 %

If the calculated ISB transmission had been used with QPSK on the first-day test, establishing a link would have not been possible for about a quarter of the time it was successful on SSB. The difference between the ITU-R channels and the calculated reference channel is not so large, as the difference is only 1 dB.

On the second testing day on November 23rd, better overall SNR levels were achieved, likely due to the high ionization of the foF2 layer. The M-class solar flares occurred at 02:59 and 14:25 UTC, which led to an Aurora Borealis visible all the way down to Southern Finland.

From Figure 38 the decline of the SNR levels after the second solar flare are evident. Soon after 15:30 UTC, the connectivity was lost, just to reappear briefly at 18:30 UTC without legible message reception. While the connection was cut off before the expected time, the results on peak SNR levels were better than on the first testing day.

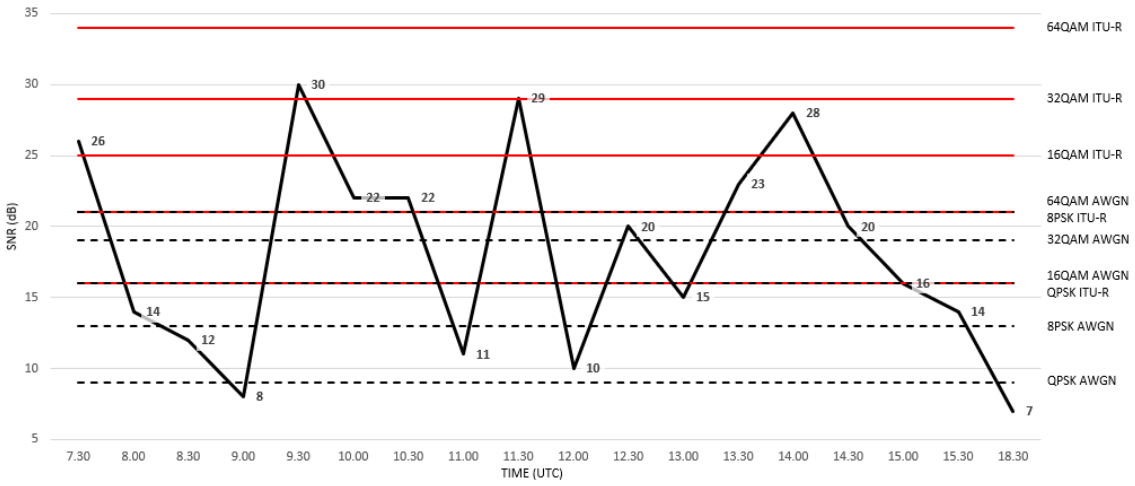

Figure 38. Measured SNR on November 23rd compared to the SNR requirements of each waveform, as defined in MIL-STD-118-110D.

While better SNR results were achieved, permitting the potential use of higher modulation, they could be interpreted worse as SNR fluctuated heavily, likely caused by fading from an enhanced D-layer, caused by solar activity. This resulted in worse conditions for communication, but better for using a higher modulation order than the previous day. Results are displayed in Table 6.

Table 6. Potential usable ISB waveforms during the November 23rd test, values for both MIL-STD-188-110D and optimally calculated half efficiency.

Waveform	MIL-STD-188-110D		Calculated (-3 dB)	
	AWGN	ITU-R	AWGN	ITU-R
QPSK	88,9 %	55,6 %	77,8 %	50 %
8PSK	72,2 %	38,9 %	55,6 %	38,9 %
16QAM	55,6 %	22,2 %	50 %	22,2 %
32QAM	50 %	11,1 %	38,9 %	5,6 %
64QAM	38,9 %	0 %	22,2 %	0 %

While the general usability worsened during the day and it would have been difficult to maintain QAM modulations, statistically an ISB QPSK would have performed slightly better than on the previous day. Overall, the day was difficult when it came to maintaining the link and while this is clear in hindsight, it would have been difficult to predict and react to at the time.

The longest maintainable high SNR levels were achieved on November 24th. The relatively stable connection between 7:00 UTC and 15:00 UTC began to degrade thereafter. Detectable SNR levels were achieved between 20:00 and 22:00 UTC, but the levels were nowhere near the earlier levels.

Another M-class solar flare occurred on the 24th at 9:17 UTC, the effects of this were not as severe as of the one the previous day. Sodankylä Geophysical Observatory's ionogram recorded a strong presence of E-layer, which had been lacking the previous days, and it likely got strengthened due to the effects of the solar flare or solar wind.

The presence of the E-layer may have been the cause for the improved RSSI, as the layer coincides with the connection time, Figure 39Figure 39. Measured SNR on November 24th compared to the SNR requirements of each waveform, as defined in MIL-STD-118-110D.. The E-layer could have reduced the

incidence angle, thus improving the gain. The short drop in SNR was caused by the spike in the noise floor, as described earlier.

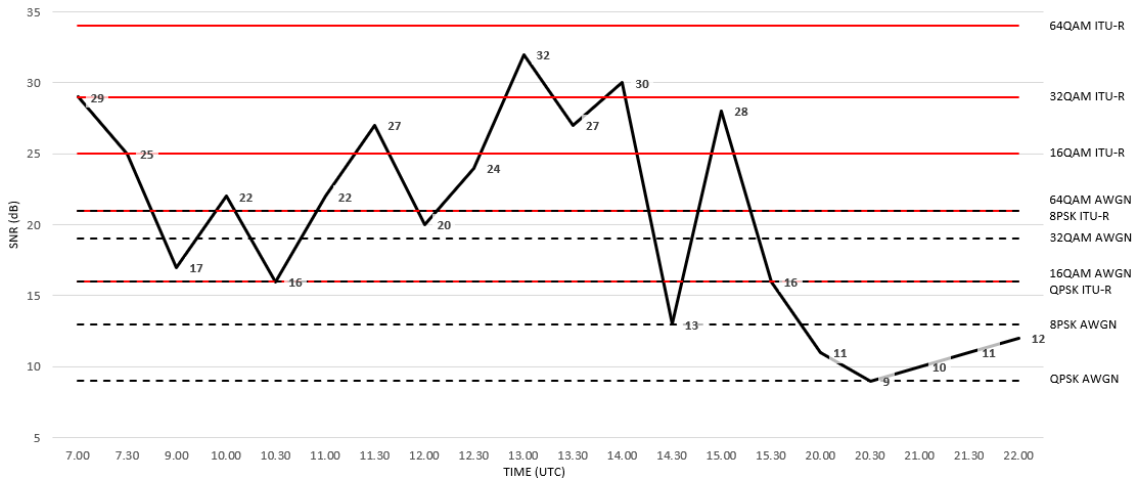

Figure 39. Measured SNR on November 24th compared to the SNR requirements of each waveform, as defined in MIL-STD-118-110D.

The SNR levels are still unsteady but able to support most of the higher QAM schemes at the estimated AWGN channel. In the ITU-R poor channel, the QPSK is the only waveform that could be considered stable. Table 7 shows that statistically QPSK and 8PSK could be estimated to be usable during the period.

Table 7. Potential usable ISB waveforms during the November 24th test, values for both MIL-STD-188-110D and optimally calculated half efficiency.

Waveform	MIL-STD-188-110D		Calculated (-3 dB)	
	AWGN	ITU-R	AWGN	ITU-R
QPSK	100 %	70 %	80 %	60 %
8PSK	75 %	50 %	70 %	50 %
16QAM	70 %	35 %	55 %	30 %
32QAM	55 %	15 %	50 %	10 %
64QAM	50 %	0 %	40 %	0 %

Solar flares likely affected the results of the first test, both positive and negative. While somewhat unexpected, they provided interesting results and variety to the first test case and highlighted the unpredictability of skywave propagation.

Some of the results can be improved by managing the frequency, but it becomes a difficult task when the link has already been lost and the change of frequency would have to be communicated. Anticipating, or predicting a sudden change in the propagation path is difficult.

Only QPSK would have been a reliable waveform for using ISB on the first test period. It is unlikely ISB waveforms would have been used, unless for ground wave propagation.

The second test was conducted on February 22nd, 2024, with more favorable ionospheric conditions. While the channel was improved, all the other settings were replicated from the previous test done in November. The period of data collection was more frequent, at 5-minute intervals.

The test period spanned from 6:00 to 14:00 UTC. During this period connectivity was maintained uninterruptedly. RSSI fluctuated between -79 and -61 dBm, with an average of -70 dBm. The noise floor was also lower, below -90 dBm, than it was in November. The overall signal levels are visible in Figure 40.

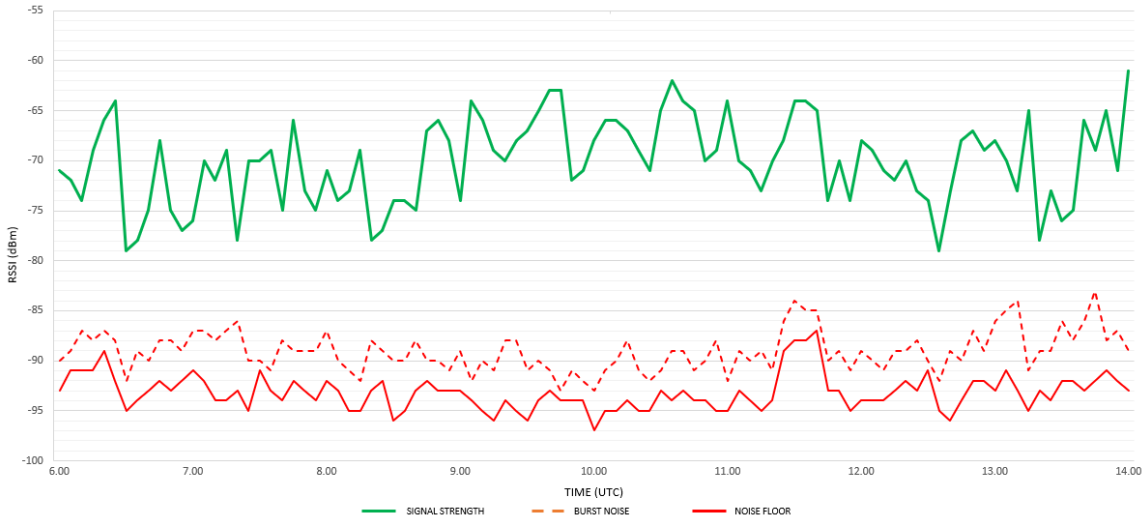

Figure 40. RSSI of QPSK SSB waveform, noise floor, and recorded burst noise levels from the second test conducted on February 22nd, 2024.

RSSI levels were fluctuating during the test due to constant fading. The RSSI level between two received transmission cycles of 1 second could be as wide as 12 dBm.

The fading was likely caused by strong solar activity on February 21st, by an X-class solar flare of magnitude X1.9, at 22:52 UTC, and on the 22nd at 6:17 UTC by another X-class of magnitude X1.7, soon after the test began. While the one happening during the test did not cause a blackout, even if the used frequency was close to the maximum usable frequency, there likely were some long-lasting effects [48, p. 2].

The SNR levels were higher than during the first test period, shown in Figure 41. The levels were still unstable due to fading, but it is easier to detect more suitable waveforms in both AWGN and ITU-R poor channel levels. The maximum SNR is 32 dB average at 23 dB, with only a few times falling as low as 15 dB.

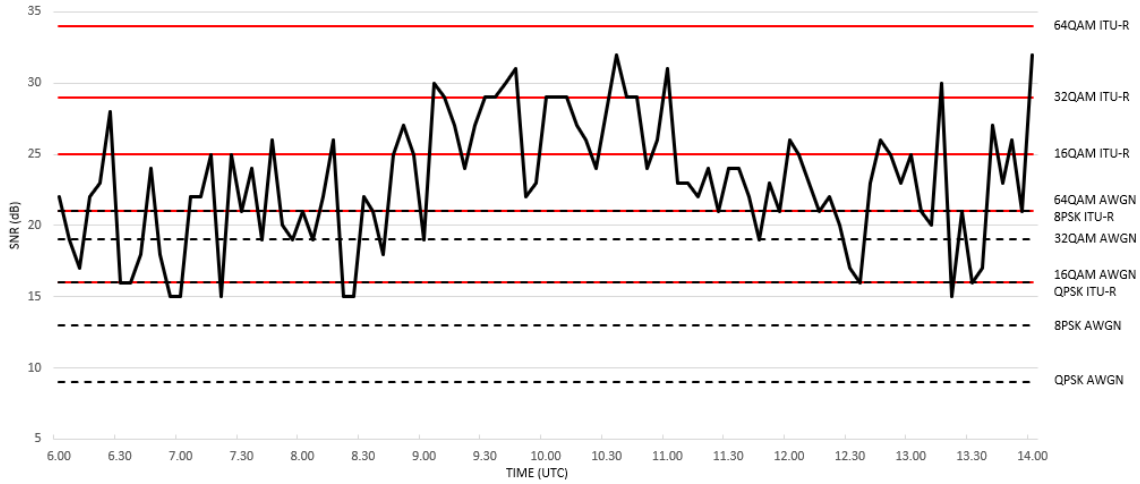

Figure 41. Measured SNR on February 22nd compared to the SNR requirements of each waveform, as defined in MIL-STD-118-110D.

All messages were received as legible during the test period, a higher modulation order would have been a valid choice. Table 8 indicates the QPSK, 8PSK, and 16QAM as usable waveforms, however, 16QAM is borderline suitable and may have not been optimal for the whole duration.

Table 8. Potential usable ISB waveforms during the February 22nd test, values for both MIL-STD-188-110D and optimally calculated half efficiency.

Waveform	MIL-STD-188-110D		Calculated (-3 dB)	
	AWGN	ITU-R	AWGN	ITU-R
QPSK	100 %	93,8 %	100 %	86,6 %
8PSK	100 %	74,2 %	89,7 %	54,6 %
16QAM	93,8 %	37,1 %	77,3 %	22,7 %
32QAM	83,5 %	15,5 %	54,6 %	4,1 %
64QAM	74,2 %	0 %	37,1 %	0 %

The results of the second test are better than those of the first test, but how much it was affected by the solar activity is difficult to say. The two X-class solar flares have had some effect; erratic fading is the likely result.

6 Conclusion

The conclusions are based on which of the waveforms are suitable for the HF tactical data link in the Finnish environment for both skywave and ground wave applications.

Based on the results of the testing, higher modulation orders are not recommended. The waveforms that would be suitable for oblique skywave communications are BPSK, QPSK, 8PSK, and 16QAM. For ground wave propagation, the 32QAM and 64QAM are better suited. The benefits compared to the UHF data rates are limited to open seas, as the gained transmission range is not comparable to other sea types.

In archipelagic environments the ground wave signal strength attenuates rapidly when propagating over land. The required SNR levels for BER $1x10^{-5}$ would likely limit the usability of 16QAM and higher waveforms. SNR can be improved by increasing the transmission power, but to a limited extent.

The advantage of ISB is the increased throughput. The required SNR for a higher modulation order in SSB is higher than at ISB. For example, the 16QAM at SSB is 4 to 6 dB higher than QPSK at ISB. The theoretical throughput is the same on these two waveforms, making ISB superior.

It could be beneficial to use π/4-QPSK instead of QPSK, as it provides robustness against fading and noise, and reduces amplitude fluctuations when transitioning to another symbol [56, p. 153].

A comprehensive channel simulation should be conducted before deeming ISB a valid option. ISB should not replace SSB completely. As seen in the test results, there are multiple cases where it is not fitting to the channel, as SSB also struggled to establish the link.

As ISB is a rare modulation in modern radio communications, it may be an expensive option to implement. The modem, radio, and tactical data link all

must support the waveform. Overall, the ISB is a good waveform option with a lower modulation order, but the suitability on QAM is unlikely and unnecessary as ISB 8PSK can reach 64QAM data rate.

The higher modulation orders could be beneficial, when combined with a cognitive SDR or other automatic network management system. Which would handle the frequency selection, based on the information collected by the radio [39, pp. 231-232].

Using SDR would remove the user agency, which can have a two-sided effect. The positive effect would be a nearly constantly working network, as the system adjusts to changing situations. The negative side is the loss of user management and therefore of situational awareness. Users become complacent when the work is done for them. The better option would be some combination of this, such as tools to estimate SNR and system recommendations based on SNR levels.

References

1 Northrop Grumman. Understanding Voice and Data Link Networking [Internet]. 2nd ed. Northrop Grumman. 2014 [cited 2023 Feb 22]. Available from: https://www.defense.info/wp-content/uploads/2018/11/Understanding_VoiceData_Link_Networking.pdf

2 Adamy D. EW 102: A Second Course in Electronic Warfare. 1st ed. Norwood, MA: Artech House; 2004. ISBN 1-58053-686-7.

3 Stallings W. Data and computer communications. 10th ed. Harlow: Pearson Education Limited; 2014. ISBN 978-1-29-201438-8.

4 Balanis CA. Antenna theory analysis and design. 4th ed. Hoboken, New Jersey: Wiley; 2016. ISBN 978-1-118-642060-1.

5 Corbac S. Electromagnetic Wave structure and parameters, vector illustration diagram with wavelength, amplitude, frequency, speed and wave types [Internet]. [cited 2023 Nov]. Available from: https://stock.adobe.com/images/electromagnetic-wave-structure-and-parameters-vector-illustration-diagram-with-wavelength-amplitude-frequency-speed-and-wave-types/310153440

6 Kennedy G, Davis B. Electronic Communication Systems. 4th ed. New Delhi: Tata McGraw-Hill; 1999. ISBN 978-0-07-463682-4.

7 Tretter S. Communications design laboratory (ENEE 428) Chapter 6: Double-Sideband Suppressed-Carrier Amplitude Modulation [Internet]. University of Maryland. 2023 [cited 2023 Nov 16]. Available from: https://user.eng.umd.edu/~tretter/commlab/c6713slides/ch6.pdf

8 Räisänen A, Lehto A. Radiotekniikan Perusteet. 12th ed. Helsinki: Hakapaino; 2007. ISBN 978-951-672-353-5.

9 Cartoonman. Link-11 [Internet]. Signal Identification Wiki. 2016 [cited 2023 Nov 18]. Available from: https://www.sigidwiki.com/wiki/File:Link-11Waterfall.png

10 Ziemer R, Tranter W. Principles of Communication: Systems, Modulation, and Noise. 7th ed. Hoboken, New Jersey: Wiley; 2014. ISBN 978-1-118-07891-4.

11 Rohde & Schwarz. Understanding Single Sideband [Internet]. www.youtube.com. 2020 [cited 2023 Dec 1]. Available from: https://www.youtube.com/watch?v=sv1xzlBut1I

12 KarapuZ. Modernised High Frequency Communication System [Internet]. Signal Identification Wiki. 2015 [cited 2023 Dec 10]. Available from: https://www.sigidwiki.com/wiki/File:Hdsdr_18858_khz.jpg

13 Department of Defense. MIL-STD-188-141D: Interoperability and Performance Standards for Medium and High Frequency Radio Systems [Internet]. Department of Defense; 2017 [cited 2023]. Available from: http://tracebase.nmsu.edu/hf/MIL-STD-188-141D.pdf

14 Department of Defense. MIL-STD-188-110D: Interoperability and Performance Standards for Data Modems [Internet]. Department of Defense; 2017 [cited 2023]. Available from: http://tracebase.nmsu.edu/hf/MIL-STD-188-110D.pdf

15 Eklöf K, Markku A, Railo K, Vermasvuori J. Radiotekniikan Perusteet. 1st ed. Vantaa: Dark; 2004. ISBN 952-13-0644-0.

16 Zeytinoglu M. ELE 635 Communication Systems: Amplitude Modulation [Internet]. Toronto Metropolitan University. 2013 [cited 2023 Dec 17]. Available from: https://www.ecb.torontomu.ca/~fernando/ELE635/Course%20Notes%20AM%20Ch4.pdf

17 Adamy D. EW 101: A First Course in Electronic Warfare. 1st ed. Norwood, MA: Artech House; 2001. ISBN 1-58053-169-5.

18 International Telecommunication Union. ITU-R P.372-16 Radio Noise [Internet]. 21st ed. Geneva: International Telecommunication Union; 2022 [cited 2023 Sep 10]. Available from: https://www.itu.int/dms_pubrec/itu-r/rec/p/R-REC-P.372-16-202208-I!!PDF-E.pdf

19 Northrop Grumman. Link 22 Guidebook Overview [Internet]. 2nd ed. San Diego: NILE Project Management Office; 2010 [cited 2023 Oct 16]. Available from: https://www.yumpu.com/en/document/read/41371305/link-22-guidebook-overview-july-2010-second-edition

20 Jones E. Basics of Radio Wave Propagation [Internet]. ecjones.org. 2000 [cited 2023 Oct 16]. Available from: http://ecjones.org/propag.html

21 U.S. Navy. Radioman 3 & 2 [Internet]. 5th ed. Washington D.C.: Training Publications Division of the Naval Personnel Program Support Activity; 1967 [cited 2023 Oct 16]. Available from: https://www.navy-radio.com/manuals/rm32-10228E-1967.pdf

22 U.S. Department of Commerce: Bureau of Navigation. Radio Service Bulletin 72 [Internet]. 1923 [cited 2023 Oct 17]. Available from: https://archive.org/details/fcc_DOC-338247A1

23 Denisowski P. The Rebirth of HF [Internet]. Rohde & Schwarz. 2020 [cited 2024 Mar 9]. Available from: https://cdn.rohde-schwarz.com/pws/campaigns/rsa/Rohde-Schwarz_Rebirth-of-HF_WhitePaper.pdf

24 Vartiainen J, Pirinen P, Vuohtoniemi R. Cognitive HF communication system with adaptive complementary codes. In: 2016 Eight International

Conference on Ubiquitous and Future Networks (ICUFN) [Internet]. IEEE; 2016 [cited 2023 Oct 18]. p. 319–321. Available from: https://ieeexplore.ieee.org/document/7537040

25 Räisänen A, Lehto A. Radiotekniikka. 7th ed. Helsinki: Otatieto; 1996. ISBN 951-672-224-5.

26 Maslin N. HF Communications: A System Approach. 1st ed. London: Pitman Publishing; 1987. ISBN 0-273-02675-5.

27 Ling R, Scholler J, Ufimtsev P. The Propagation and Excitation of Surface Waves in an Absorbing Layer. Progress In Electromagnetics Research [Internet]. 1998 Jan 1 [cited 2023 Oct 18]; Vol 19: 49–91. Available from: https://www.jpier.org/PIER/pier.php?paper=970718

28 Angulo I, Barclay L, Chernov Y, Deminco N, Fernández I, Gil U, et al. Handbook on Ground Wave Propagation [Internet]. International Telecommunication Union; 2014 [cited 2023 Oct 4]. Available from: https://www.itu.int/dms_pub/itu-r/opb/hdb/R-HDB-59-2014-PDF-E.pdf

29 Eckert R. Modern Methods for Calculating Ground-Wave Field Strength Over A Smooth Spherical Earth [Internet]. Federal Communication Commission; 1986 [cited 2023 Oct 20]. Available from: https://transition.fcc.gov/bureaus/oet/info/documents/reports/oet_r86-1.pdf

30 Suomen ympäristökeskus. The Marine Data Portal [Internet]. Itämeri.fi. 2020 [cited 2023 Oct 21]. Available from: https://merihavainnot.ymparisto.fi/merihavainnot/

31 Noah M. Ground-Wave Propagation, Earth Surface Dielectric Properties [Internet]. MathWorks. 2023 [cited 2023 Oct 20]. Available from: https://se.mathworks.com/matlabcentral/fileexchange/89546-ground-wave-propagation-earth-surface-dielectric-properties/

32 Lindell I. Radioaaltojen eteneminen. 5th ed. Helsinki: Otatieto; 2000. ISBN 951-672-227-X.

33 International Telecommunication Union. ITU-R P.368-10: Ground-wave propagation prediction method for frequencies between 10 kHz and 30 MHz [Internet]. International Telecommunication Union; 2022 [cited 2023 Oct 25]. Available from: https://www.itu.int/dms_pubrec/itu-r/rec/p/R-REC-P.368-10-202208-I!!PDF-E.pdf

34 Levent S. Groundwave Modeling and Simulation Strategies and Path Loss Prediction Virtual Tools. IEEE Transactions on Antennas and Propagation [Internet]. 2007 Jun 11 [cited 2023 Oct 25];55(6):1591–1598. Available from: https://ieeexplore.ieee.org/document/4232654

35 Blaunstein N, Christodoulou C. Radio Propagation and Adaptive Antennas for Wireless Communication Links. 1st ed. Hoboken: Wiley; 2007. ISBN 978-0-470-06998-1.

36 Barrick D. Theory of HF and VHF Propagation Across the Rough Sea, 2, Application to HF and VHF Propagation Above the Sea. Radio Science [Internet]. 1971 May [cited 2023 Oct 28];6(5):527–533. Available from: https://ieeexplore.ieee.org/document/7773187

37 Davila C. Comparison of HF groundwave propagation models [Internet] [Thesis]. [United States Navy, Naval postgraduate school]; 1993 [cited 2023 Nov 3]. Available from: https://apps.dtic.mil/sti/tr/pdf/ADA273146.pdf

38 Hufford G. The ITS Irregular Terrain Model, version 1.2.2 - The Algorithm [Internet]. Institute for Telecommunication Sciences. 1999 [cited 2023 Nov 3]. Available from: https://www.its.ntia.gov/umbraco/surface/download/publication?reportNumber=HuffordITMalgWhitePaper.pdf

39 Johnson E, Koski E, Furman W, Jorgenson M, Nieto J. Third-generation and wideband HF radio communications. 1st ed. Norwood, MA: Artech House; 2013. ISBN 978-1-60807-503-4.

40 Greiner G. Shortwave Communication. Berlin: Fachverlag Schiele & Schön GmbH; 1990.

41 Harden P. Solar Activity & HF Propagation. In: Four Days In May (FDIM) [Internet]. Dayton: Amateur Radio Club International; 2005 [cited 2024 Jan 2]. Available from: https://www.qrparci.org/resource/FDIM81.pdf

42 Australian Bureau of Meteorology. HF Radio Propagation. Surry Hills: Australian Bureau of Meteorology - Space Weather Services; 2016.

43 Zolesi B, Cander L. Ionospheric Prediction and Forecasting [Internet]. Heidelberg: Springer Science & Business Media; 2013. ISBN 978-3-642-38429-5. Available from: https://link.springer.com/book/10.1007/978-3-642-38430-1

44 Lee J. An Introduction to Radio Wave Propagation. 1st ed. London: Bernard Babani (publishing) Ltd.; 1991. ISBN 0-85934-238-7.

45 Straw R, Andress K, Cebik L, Severns R, Witt F. The ARRL Antenna Book. 19th ed. Newington: The American Radio Relay League; 2000. ISBN 978-0872598041.

46 Denisowski P. Educational Note: Understanding NVIS [Internet]. Rohde & Schwarz. 2020 Jul [cited 2024 Jan 6]. Available from: https://cdn.rohde-schwarz.com/pws/campaigns/rsa/Rohde-Schwarz_Understanding-NVIS_v1.1.pdf

47 National Oceanic and Atmospheric Administration. Solar Cycle Progression [Internet]. Space Weather Prediction Center. 2024 [cited 2024 Jan 1]. Available from: https://www.swpc.noaa.gov/products/solar-cycle-progression

48 Fiori R, Kumar V, Boteler D, Terkildsen M. Occurrence rate and duration of space weather impacts on high-frequency radio communication used by aviation. Journal of Space Weather and Space Climate [Internet]. 2022 [cited 2024 Jan 7];12(21). Available from: https://www.swsc-journal.org/articles/swsc/pdf/2022/01/swsc220003.pdf

49 Sodankylä Geophysical Observatory. SGO Real-time Data: Ionogram [Internet]. www.sgo.fi. 2024 [cited 2024 Jan 8]. Available from: https://www.sgo.fi/Data/RealTime/ionogram.php

50 Zawdie K, Drob D, Siskind D, Coker C. Calculating the absorption of HF radio waves in the ionosphere. Radio Science [Internet]. 2017 Jun [cited 2024 Jan 10];52(6):767–783. Available from: https://agupubs.onlinelibrary.wiley.com/doi/epdf/10.1002/2017RS006256

51 International Telecommunication Union. ITU-R F.1487: Testing of HF modems with bandwidths of up to about 12 kHz using ionospheric channel simulators [Internet]. International Telecommunication Union. 2000 [cited 2024 Jan 11]. Available from: https://www.itu.int/dms_pubrec/itu-r/rec/f/R-REC-F.1487-0-200005-I!!PDF-E.pdf

52 Bradley P, Hanbaba R, Cole D, Barclay L, Belrose J, Davey I, et al. ITU-R Handbook: The Ionosphere and Its Effects on Radiowave Propagation [Internet]. International Telecommunication Union; 1998. Available from: https://www.itu.int/dms_pub/itu-r/opb/hdb/R-HDB-32-1998-PDF-E.pdf

53 Zhu W, Guo L, He S. Analysis of HF receiving Antenna SNR and Application. Radio Science [Internet]. 2022 Jan 1 [cited 2024 Jan 13];57(1). Available from: https://agupubs.onlinelibrary.wiley.com/doi/epdf/10.1029/2021RS007343

54 Pozar D. Microwave Engineering. 4th ed. Hoboken: Wiley; 2012. ISBN 978-0-470-63155-3.

55 Watterson C, Juroshek J, Bensema W. Experimental Confirmation of an HF Channel Model. IEEE Transactions on Communications Technology [Internet]. 1970 Dec [cited 2024 Jan 16];18(6):792–803. Available from: https://ieeexplore.ieee.org/document/1090438

56 Goldsmith A. Wireless communications. Cambridge: Cambridge University Press; 2005. ISBN 978-0-511-13675-7.

57 International Telecommunication Union. Recommendation F.520-2: Use of high frequency ionospheric channel simulators (withdrawn) [Internet]. International Telecommunication Union. 1992 [cited 2024 Feb 3]. Available from: https://www.itu.int/dms_pubrec/itu-r/rec/f/R-REC-F.520-2-199203-W!!PDF-E.pdf

58 National Oceanic & Atmospheric Administration. The aurora and solar activity archive: November 23rd, 2023 [Internet]. SpaceWeatherLive.com.

2023 [cited 2024 Feb 15]. Available from: https://www.spaceweatherlive.com/en/archive/2023/11/23/xray.html

Ionospheric conditions during the testing periods

This appendix contains the recorded ionospheric and solar data during the testing period, as reported by Sodankylä Geophysical Observatory (SGO) and SpaceWeatherLive.com retrieved from the National Oceanic and Atmospheric Administration (NOAA) data.

1. November 22nd, 2023

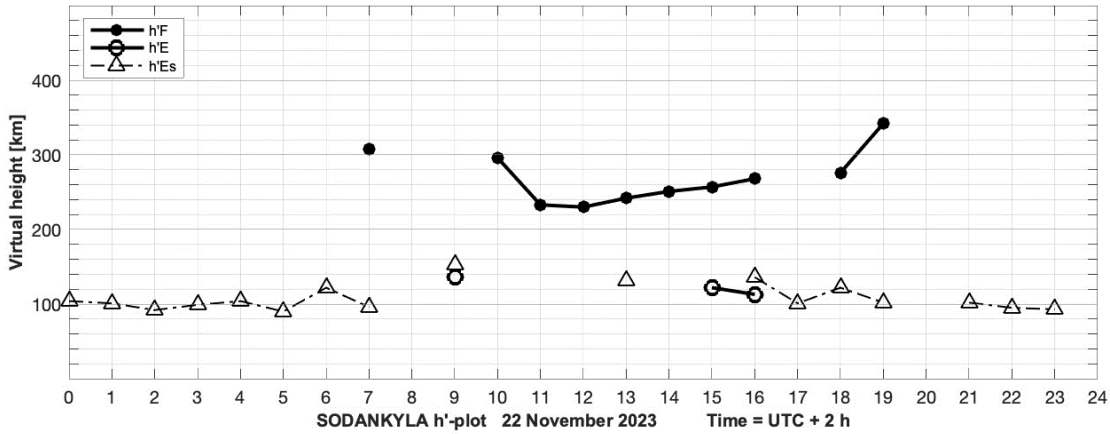

Figure 1. Virtual height of the ionospheric layers F, E, and E_s. Measured by SGO, Northern Finland. foF2 is detected only between 8:00 to 14:00 UTC, while foE_s have dominated most of the evening and nighttime. The link was established after 14:00, but SNR was not steady.

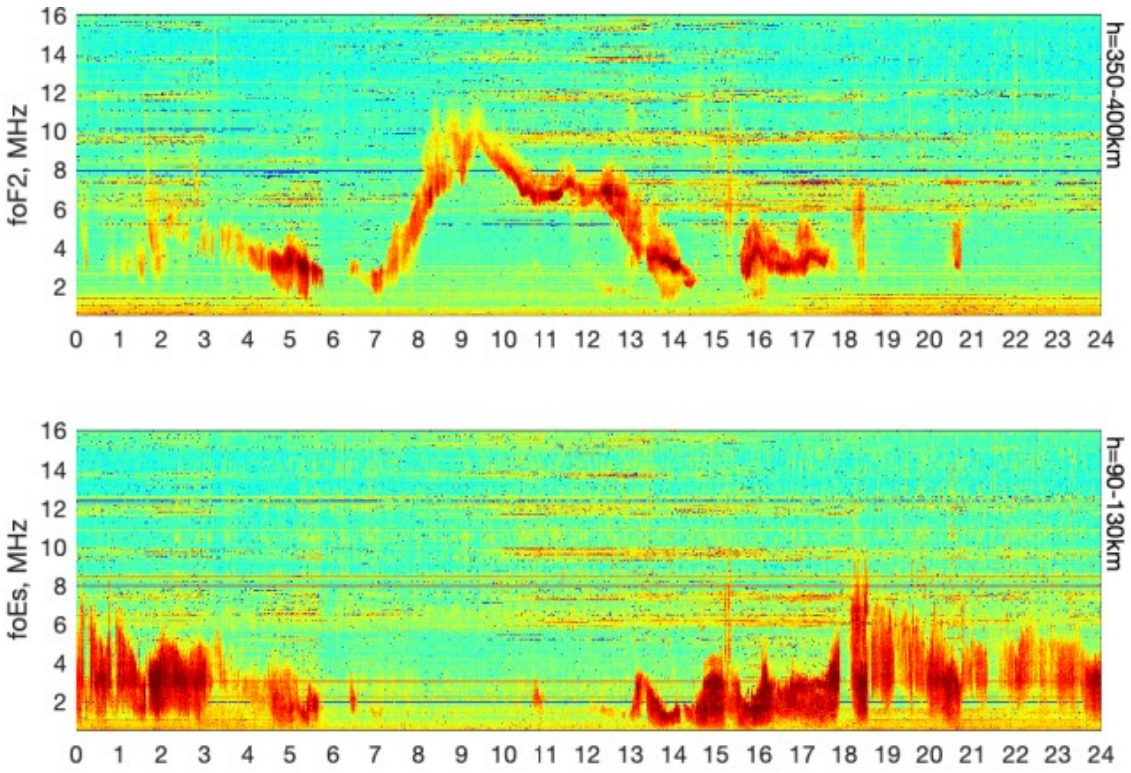

Figure 2. Detected critical frequency of foF2 and foEs, the time zone is UTC +2. Measured by SGO, Northern Finland. During most of the daytime, the critical frequency was between 6 to 8 MHz. Strong foE_s is present from midnight to 3:00 and appear again at 15:00.

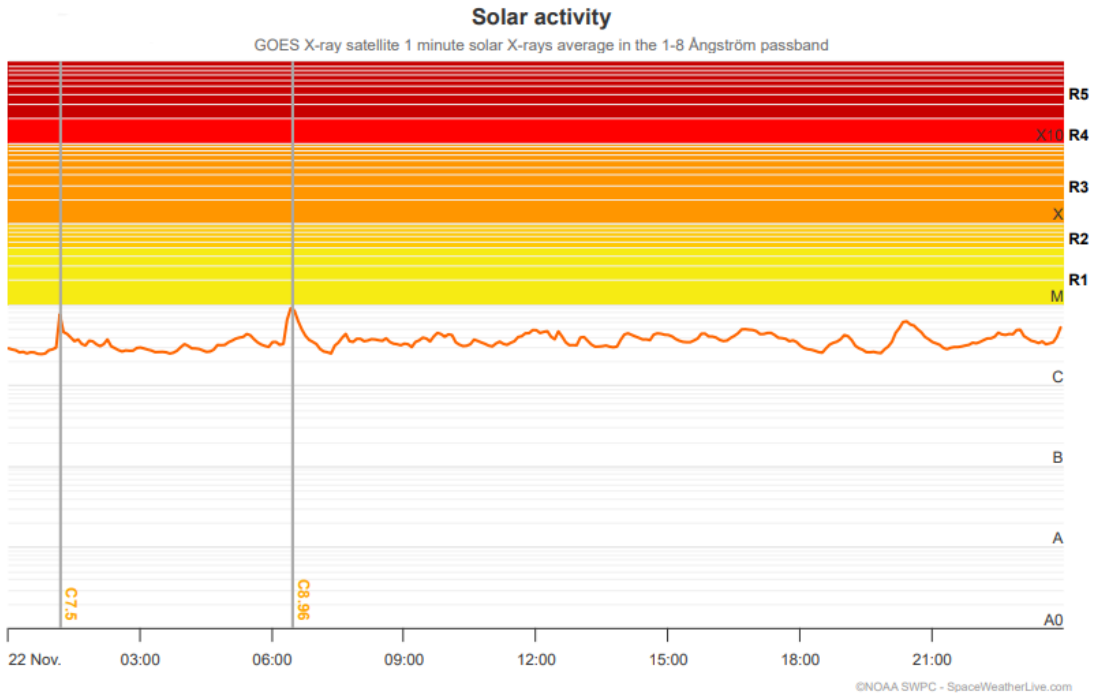

Figure 3. Solar flare activity. Measured by NOAA and collated by SpaceWeatherLive.com. Activity is calm; only two C-class solar flares of magnitude C7.5 and C8.96, have little to no effect on the ionosphere.

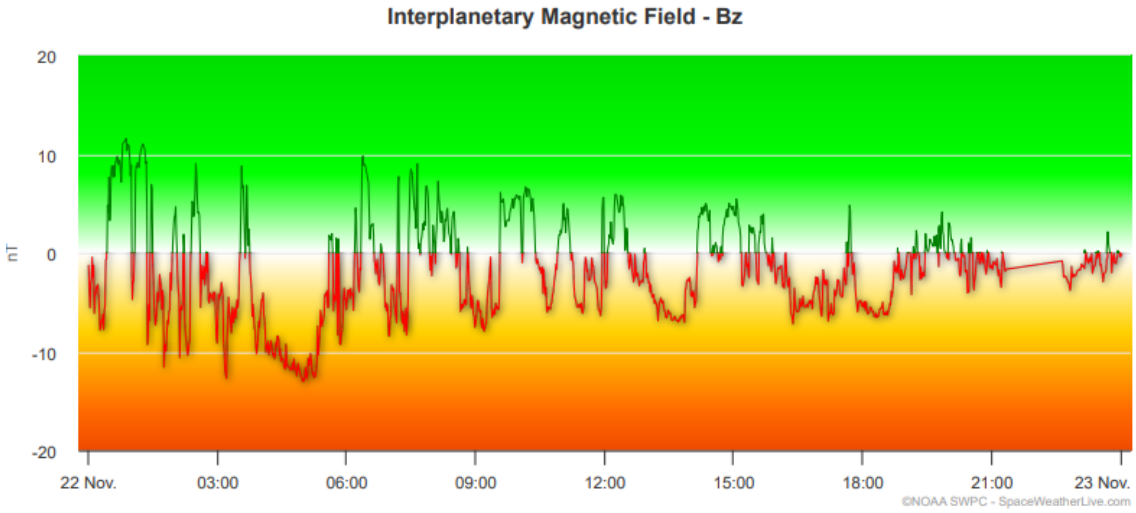

Figure 4. Solar wind's interaction with Earth's magnetosphere at the polar axis (Bz). Measured by NOAA and collated by SpaceWeatherLive.com. Values below -10 nT indicate a possibility for a geomagnetic storm.

2. November 23rd, 2023

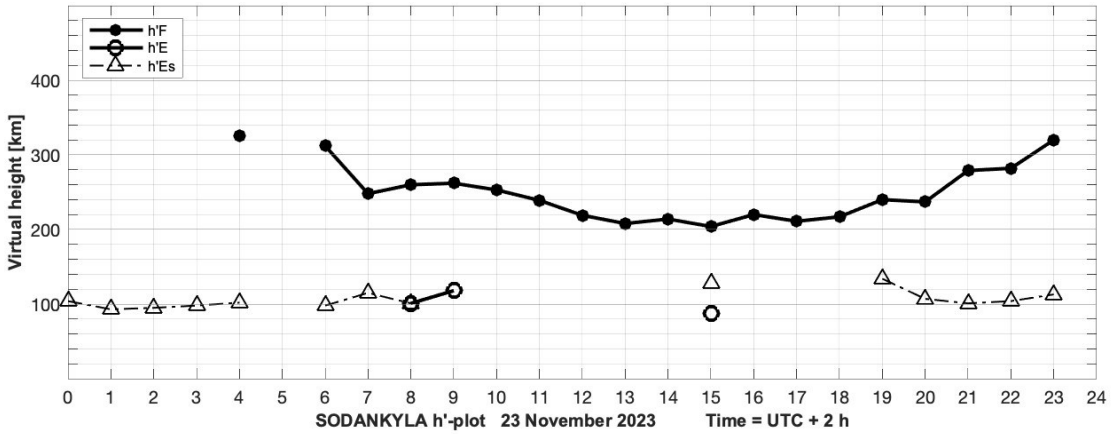

Figure 5. Virtual height of the ionospheric layers F, E, and E_s. Measured by SGO, Northern Finland. foF2 was detected throughout the whole day, until late evening.

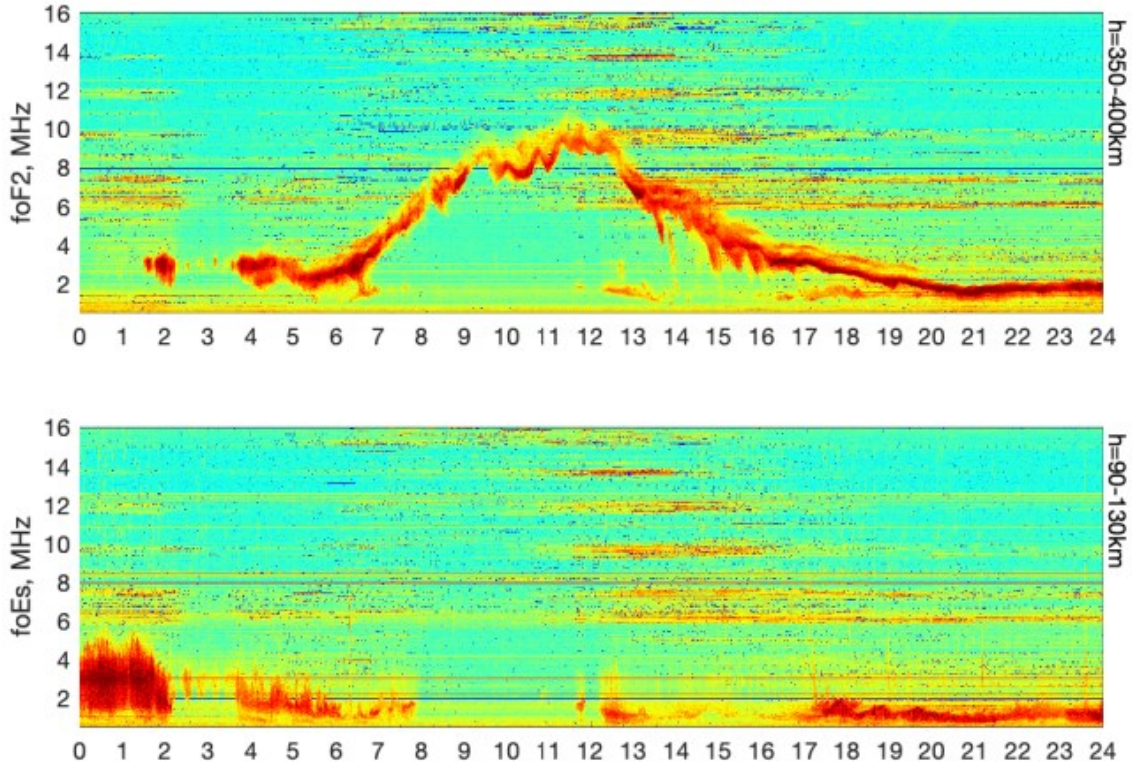

Figure 6. Detected critical frequency of foF2 and foEs, the time zone is UTC +2. Measured by SGO, Northern Finland. During most of the daytime, the critical frequency has been between 7 to 10 MHz. foE_s is present from 17:00 on, but nowhere near as strong as the previous day.

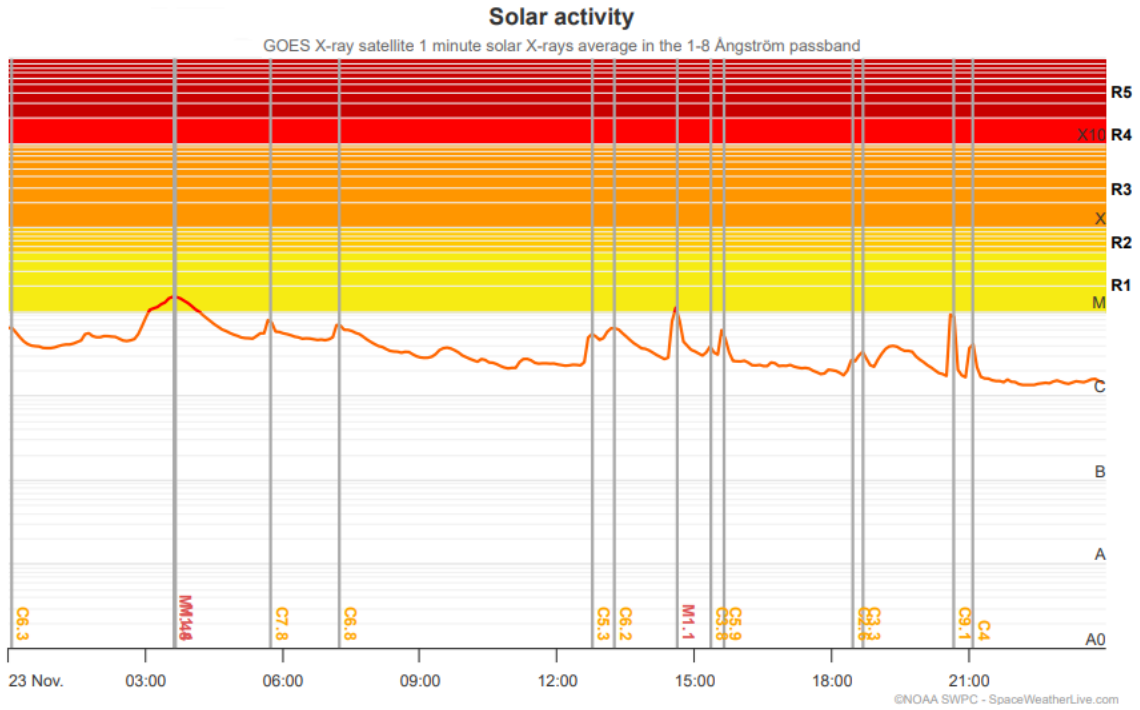

Figure 7. Solar flare activity. Measured by NOAA and collated by SpaceWeatherLive.com. Activity has increased; two M-class solar flares of magnitude M1.48 and M1.1, which can have influenced the ionosphere and caused short blackouts on HF communication on the dayside.

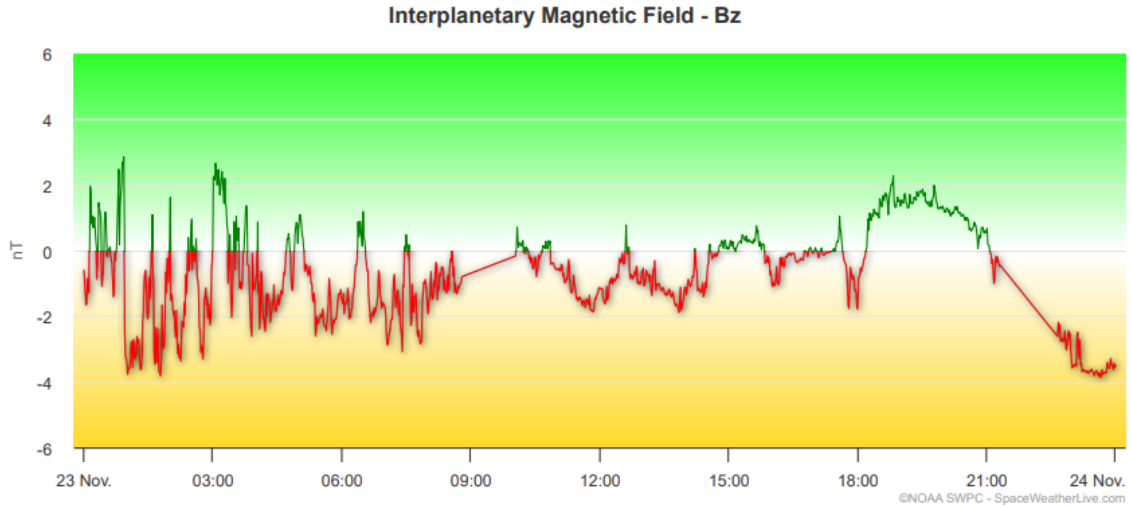

Figure 8. Solar wind's interaction with Earth's magnetosphere at the polar axis (Bz). Measured by NOAA and collated by SpaceWeatherLive.com. No effect on the magnetosphere.

3. November 24th, 2023

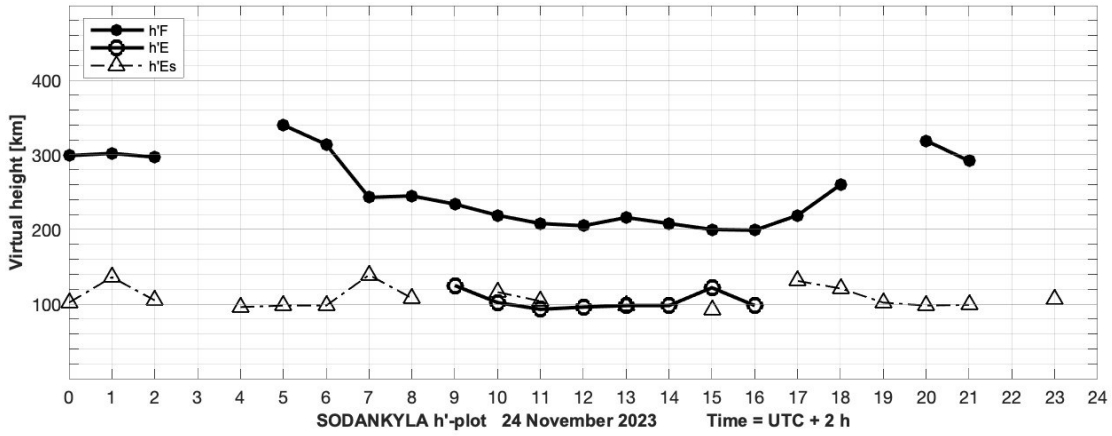

Figure 9. Virtual height of the ionospheric layers F, E, and Es. Measured by SGO, Northern Finland. foF2 was detected throughout the whole daytime and foE was detected as well, unlike in the previous days.

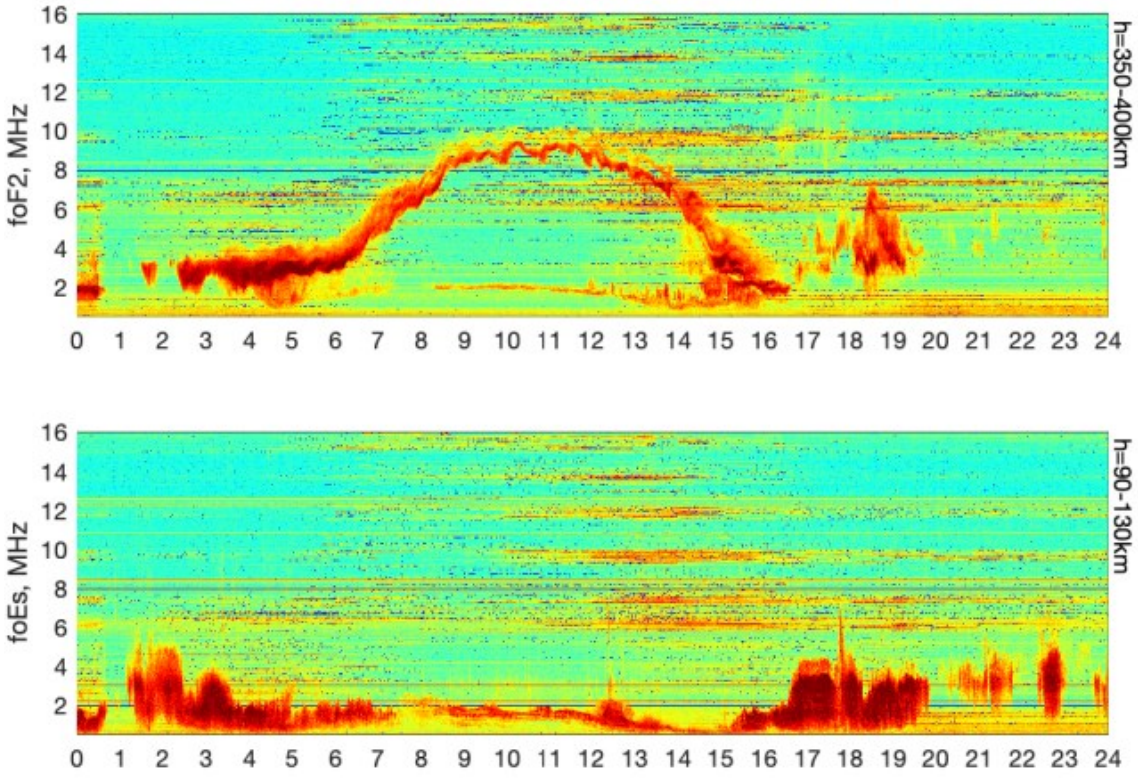

Figure 10. Detected critical frequency of foF2 and foE_s, the time zone is UTC +2. Measured by SGO, Northern Finland. During most of the daytime, the critical frequency has been between 6 to 9 MHz, spanning longer periods than during the previous days. foE_s is present the whole day and foE was detected from 8:00 to 16:00.

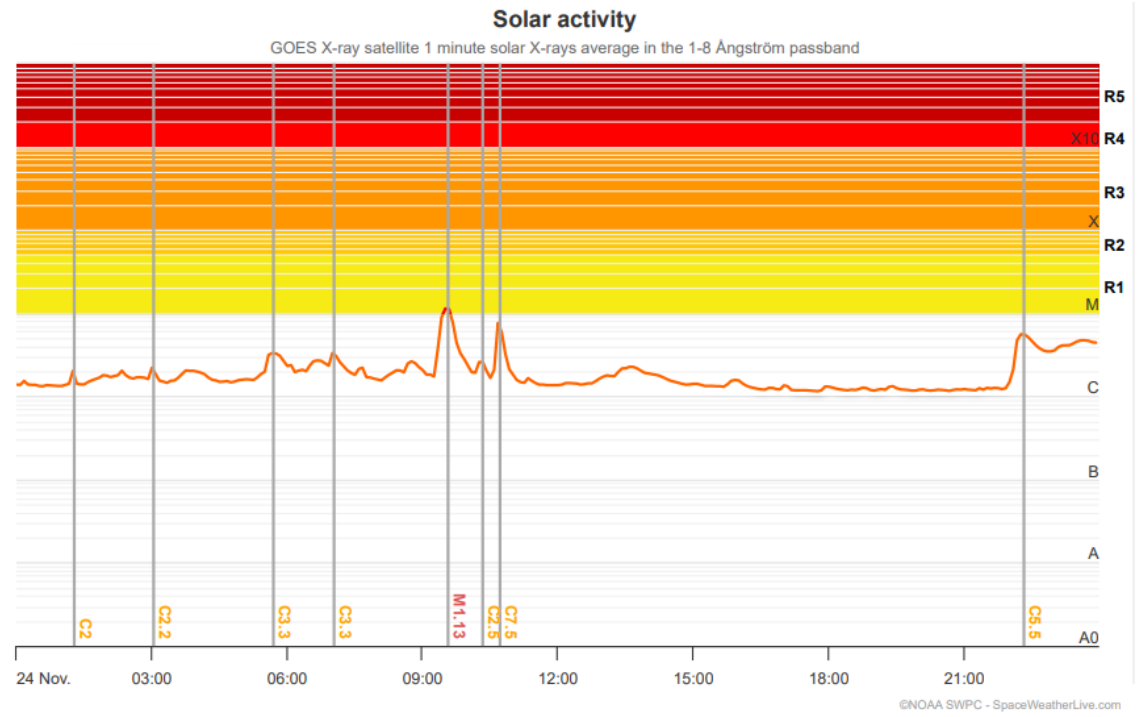

Figure 11. Solar flare activity. Measured by NOAA and collated by SpaceWeatherLive.com. Single M-class solar flares of magnitude M1.13, which may have affected the ionosphere. No HF blackout was observed during the test.

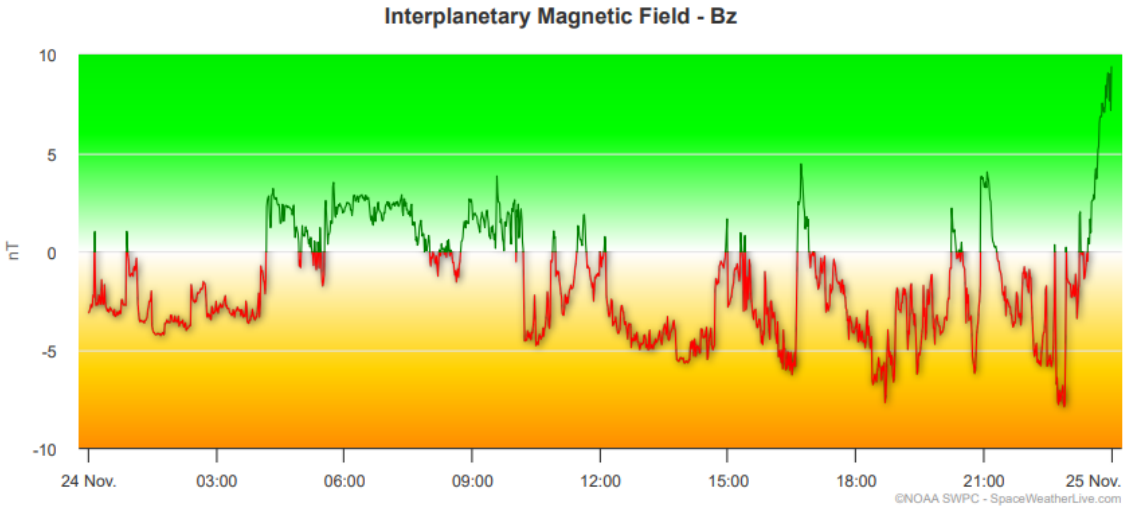

Figure 12. Solar wind's interaction with Earth's magnetosphere at the polar axis (Bz). Measured by NOAA and collated by SpaceWeatherLive.com. While the recorded fluctuation is higher than the previous day, it likely had little to no effect.

4. February 22nd, 2024

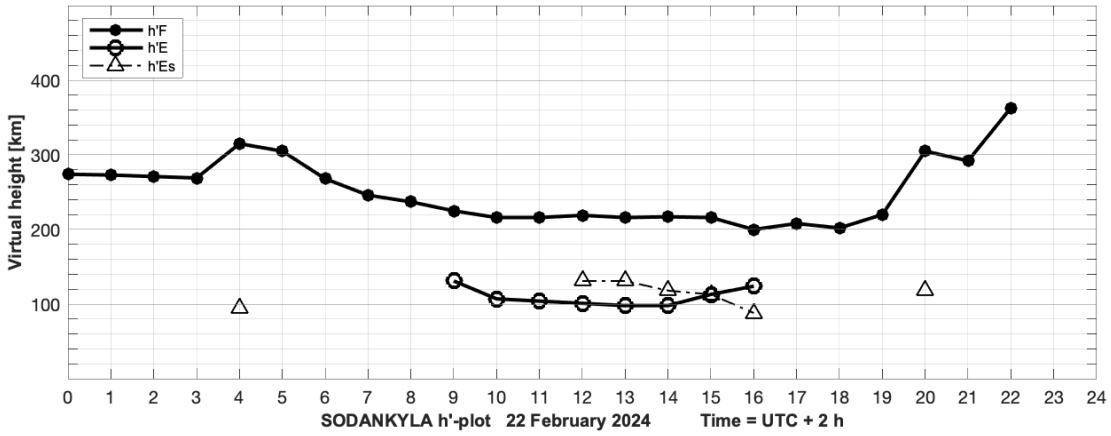

Figure 13. Virtual height of the ionospheric layers F, E, and Es. Measured by SGO, Northern Finland. foF2 was detected throughout the whole day. The detectable presence of foF2 during the nighttime is likely caused by the high solar activity during this period.

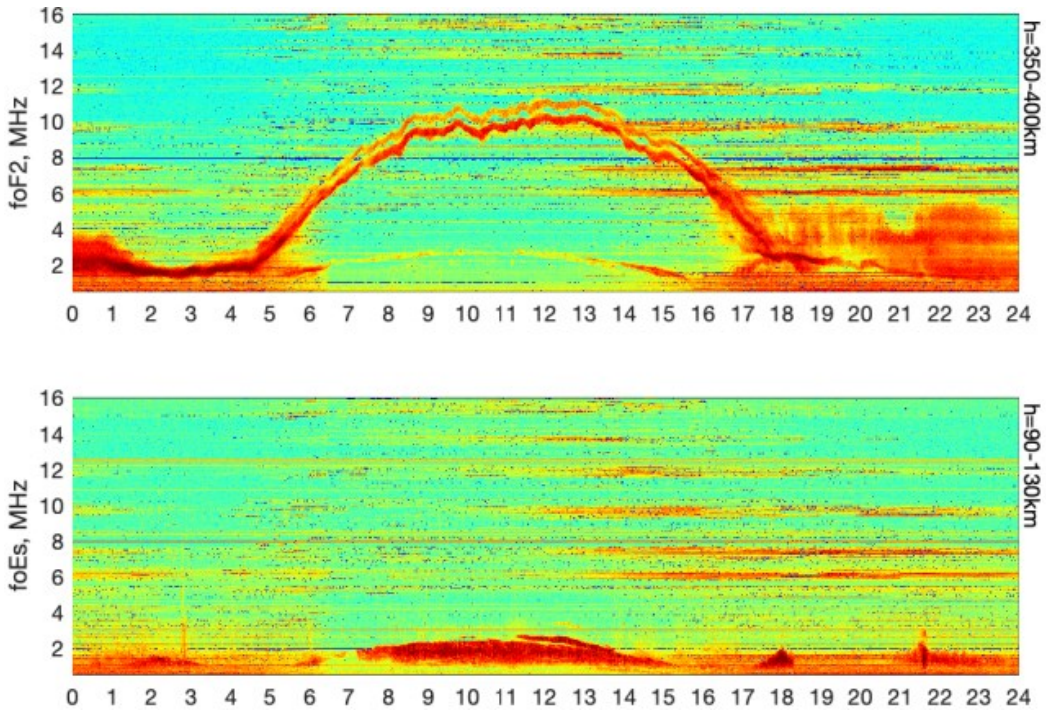

Figure 14. Detected critical frequency of foF2 and foEs, the time zone is UTC +2. Measured by SGO, Northern Finland. During most of the daytime, the critical frequency has been between 8 to 10 MHz.

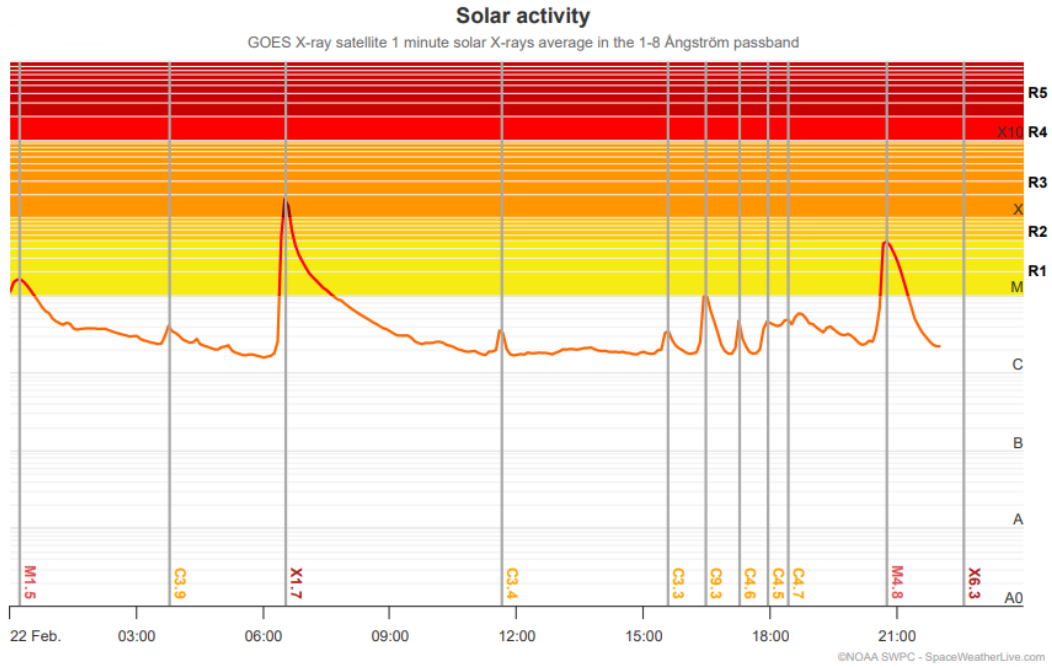

Figure 15. Solar flare activity. Measured by NOAA and collated by SpaceWeatherLive.com. Two X-class solar flares of magnitude X1.7 and X6.3, of which the first during the test. No HF blackout was observed during the test.

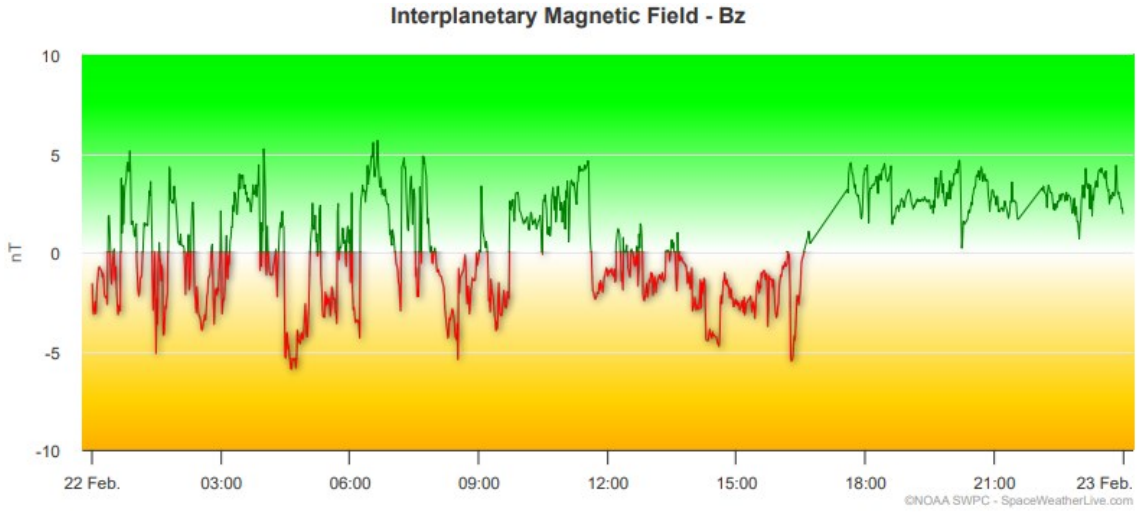

Figure 16. Solar wind's interaction with Earth's magnetosphere at the polar axis (Bz). Measured by NOAA and collated by SpaceWeatherLive.com. No effect on the magnetosphere.

Radio power output measurement

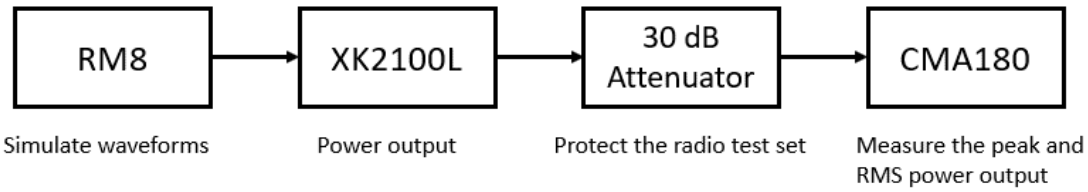

Figure 1. Radio power output measurement setup. Below the block diagram are descriptions of each block's task.

Table 1. The measured power output values are compared to the values in the official datasheet. These values account for the 30 dB attenuator.

Power setting	Datasheet (W)	Peak (dBm)	RMS (dBm)	Peak (W)	RMS (W)
Low	10	42.4	37	16.6	5
Medium	30	48.8	41.4	75.9	13.8
High	100	52.2	46.5	166	44.7